JPhys Energy

TOPICAL REVIEW • OPEN ACCESS

Catalytic reactions for H_2 production on multimetallic surfaces: a review

IOP Publishing J. Phys. Energy 3 (2021) 032016 https://doi.org/10.1088/2515-7655/ac0d9f

Journal of Physics: Energy

TOPICAL REVIEW

Catalytic reactions for H_2 production on multimetallic surfaces: a review

Rui V Afonso[1], José D Gouveia[1] and José R B Gomes[*]

CICECO—Aveiro Institute of Materials, Department of Chemistry, University of Aveiro, Campus Universitário de Santiago, 3810-193 Aveiro, Portugal

[1] Equal Contribution.

[*] Author to whom any correspondence should be addressed.

E-mail: jrgomes@ua.pt

Keywords: H_2 production, water–gas shift reaction, steam reforming, ammonia decomposition, methanol decomposition, multimetallic surfaces, heterogeneous catalysis

OPEN ACCESS

RECEIVED
31 December 2020

REVISED
25 March 2021

ACCEPTED FOR PUBLICATION
22 June 2021

PUBLISHED
14 July 2021

Abstract

Herewith, an overview is provided on the recent developments in the utilization of multimetallic catalysts to produce large amounts of molecular hydrogen, especially via the steam reforming of hydrocarbons and the water–gas shift reaction. Emphasis is given on the explanation of the problems affecting the currently used catalysts and how the addition/incorporation of other metals in available or new catalysts may lead to improved catalyst activity, selectivity and stability. We compare results from selected key examples taken from the literature where multimetallic catalysts are used for the aforementioned reactions. The methanol and ammonia decompositions are also critically analyzed, with focus on Earth-abundant metal elements.

1. Introduction

The potential of molecular hydrogen (H_2) as an energy carrier is expected to play a crucial role in future energy systems. Hydrogen can be obtained from renewable and nonrenewable sources, with different colors unofficially assigned by the North American Council for Freight Efficiency (NACFE [1]) to denote hydrogen origin. Renewable (green) hydrogen can be obtained, e.g. from water splitting into hydrogen and oxygen in an electrolyzer that is fed with renewable electricity from wind or solar farms, or from the steam reforming of inedible or waste biomass. Red/yellow hydrogen is produced by the electrolysis of water with nuclear power/grid electricity and turquoise hydrogen is produced from methane pyrolysis. Nevertheless, at present, the major fractions of the World's hydrogen arise from the steam methane reforming of natural gas or oil/naphta (78%, gray hydrogen) and from coal gasification (18%, brown hydrogen), figure 1.

As can be seen in figure 1, a successful combination of steam reforming of natural gas and water gas shift reactions will lead mostly to hydrogen gas and carbon dioxide, with the former being then used as a fuel and with the latter being (a) released to the atmosphere (eventually recycled through the natural plant respiration cycle to generate biomass), (b) used in alternative chemical processes (e.g. as an oxidant weaker than O_2 or C_1-building block to obtain high-value chemicals), (c) sequestered by suitable underground geologic formations, or (d) repurposed for CO_2 enhanced oil recovery processes [2, 3]. According to the NACFE coloring code, hydrogen from gray/brown sources but with CO_2 effectively repurposed/sequestered takes the blue color. The importance of the reforming of biomass is expected to increase significantly in forested areas since it may allow for nearly carbon neutral processes, which is of utmost importance to counter the global warming.

For hydrogen to become a viable fuel option, greater quantities must be produced cleanly and efficiently, and production costs must be lowered. The implementation of the infrastructure to distribute hydrogen is greatly dependent on a steady and cost-effective hydrogen supply and several different hydrogen carriers (e.g. ammonia, methanol, toluene/methylcyclohexane pair, etc [4]) have been considered for bulk storage and transport of hydrogen. The current annual global dedicated hydrogen production is about 70 megatons but it was recently estimated that this amount will be doubled in the next 5 years [5]. To ensure these

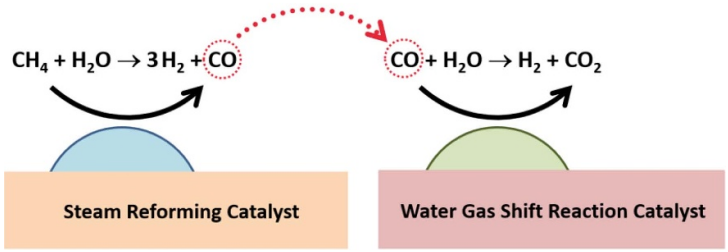

Figure 1. Schematic view of the process of steam reforming of methane (SRM) to produce H_2 and CO (on the left), with the latter being combined with steam to produce additional H_2 through the water–gas shift reaction (WGSR, on the right). The WGSR is also important to convert CO from coal gasification ($3\,C + O_2 + H_2O \rightarrow H_2 + 3CO$) to additional hydrogen. The conversion and selectivity are governed by the appropriateness of the catalysts used in each reaction.

demands can be met, catalysts that can increase the activities of the reactions used for H_2 production must be found. Such catalysts must solve the problems found with conventional metal/metal oxide support catalysts, e.g. low conversion during startup/shutdown, high energy demands, and deactivation by sintering or by poisoning species like sulfur. For compact applications, pyrophoric problems inherent to some of the available catalysts also must be solved.

Recent strategies rely on the addition of other metals to existing or to newly designed metal-based catalysts to form metallic alloys, in which synergic interactions can solve at least some of the problems referred above that are associated to current commercial catalysts. However, this is not an easy task since the nature of the metallic elements, their exact proportion in the alloy, the nature of the support, the size and shape of the metal or metal alloy particles, among many others, are all important variables that may significantly affect the catalyst activity and selectivity.

In this review, we seek to examine recent scientific advances on the application of multimetallic catalysts in the production of H_2 through the water gas shift reaction (WGSR) and the steam reforming of hydrocarbons which are the current workhorses in industry for producing large quantities of this gas. We briefly discuss why the CO_2 dry reforming of methane (DRM) is less interesting for producing H_2 than the steam reforming of methane (SRM), despite the former consuming CO_2, thus contributing to effective carbon capture. Finally, we review the importance of multimetallic catalysts in the reactions of the decomposition of methanol and ammonia to produce H_2 in more compact applications. Methanol and ammonia [6], which may be produced during periods of excess sustainable energy, are easily liquefied and, consequently, can be stored and handled more easily than liquid H_2. Given the vast literature on the field, we could not address all the works published in the literature devoted entirely to each of the individual reactions considered and we refer the reader to other excellent reviews of steam reforming of hydrocarbons [5, 7], WGSR [8], and methanol [9, 10] or ammonia decompositions [11].

2. Reactions for H_2 production

2.1. Steam reforming of hydrocarbons

2.1.1. Introduction

Steam reforming of hydrocarbons is the standard production method of hydrogen at an industrial scale [12, 13]. It follows the general reaction:

$$C_nH_m + nH_2O \rightarrow nCO + \left(\frac{m}{2} + n\right) H_2, \tag{1}$$

yielding syngas as its reaction product. The reaction always produces more H_2 than CO, with light hydrocarbons giving higher H_2 yields. For this reason, and due to lower investment costs, production of hydrogen is preferentially performed with light hydrocarbons [12, 13]. The reaction is usually realized at 700 °C–925 °C, in the presence of a catalyst [13]. A posterior stage can be employed, at somewhat lower temperatures, where the WGSR equation (2),

$$CO + H_2O \rightarrow CO_2 + H_2\,,\ \Delta H = -41\ \text{kJ mol}^{-1} \tag{2}$$

is used. The WGSR further increases H_2 yield, which is highly positive if the purpose of the process is to obtain pure H_2, and not syngas. This reaction is exothermic, which allows it to be promoted at lower temperatures than the steam reforming reaction. The steam reforming reaction proceeds entirely through the action of the catalyst; both the organic compound and water are decomposed on its surface, followed by

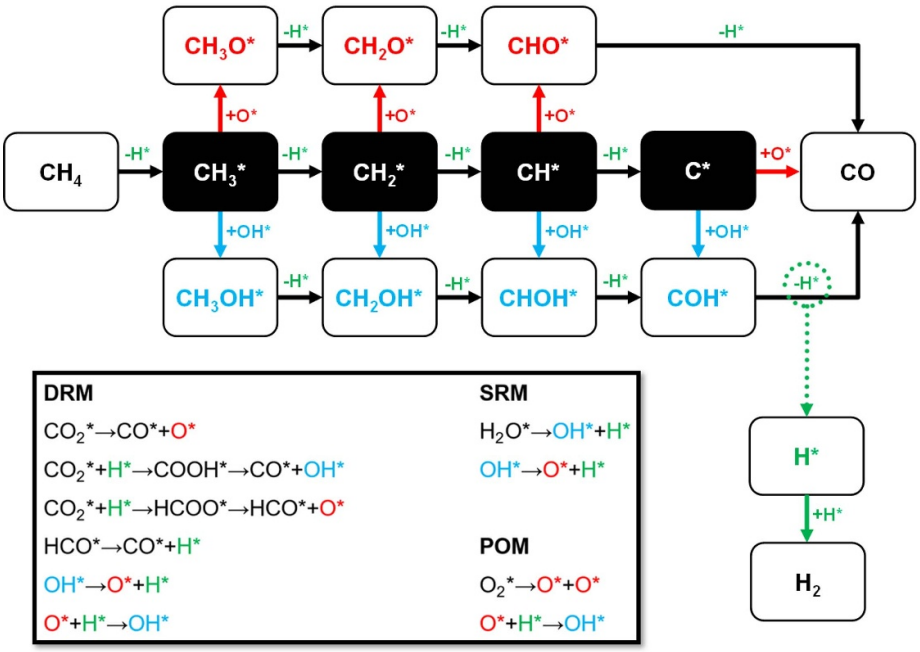

Figure 2. Decomposition sequences and formation pathways for the different products involved in H_2 production from methane. The reactions generating the oxidant species in the DRM, SRM and POM processes are also shown.

product formation and desorption. Overwhelmingly, methane (in the form of natural gas) is the hydrocarbon of choice for the production of hydrogen through steam reforming [14, 15].

Dry reforming is a potential alternative to steam reforming, for generating syngas from hydrocarbons, which uses carbon dioxide, instead of water, as a reforming reagent. Just like steam reforming, dry reforming yields syngas:

$$C_nH_m + nCO_2 \rightarrow 2nCO + \frac{m}{2}H_2. \quad (3)$$

Unlike steam reforming, dry reforming typically yields more CO than H_2. It is thus more adequate for applications where the purpose is production of synthesis gas, and not pure H_2. DRM yields syngas in a 1:1 ratio. This ratio can be adjusted at a posterior stage, if necessary, although this incurs a cost [16]. Heavier hydrocarbons carry the problem of increased coke formation [17], which is a common occurrence with natural gas and biogas feeds [12]. Methane is thus the preferential hydrocarbon used in dry reforming processes. With two carbon sources instead of one, the tendency for carbon deposition is much higher in DRM than in steam reforming [18]. Furthermore, unlike with steam reforming, a high CO_2/CH_4 ratio does not help in this situation. In fact, steam may be used as an additive in dry reforming, so as to prevent coking [19]. Since the dry reforming of hydrocarbons is less appropriate for H_2 production than the steam reforming, this process will not be reviewed here. Yet, recent accounts about multimetallic catalyst design for the DRM can be found in the literature [20–23].

2.1.2. Monometallic catalysts

Methane steam reforming is usually conducted using a nickel catalyst supported on Al_2O_3 or SiO_2 [12, 14, 15, 24, 25]. Even though nickel is known to not be the most active element for this reaction [26], it has the advantage of being a relatively cheap transition metal (TM), giving a good compromise between stability, activity and cost [25, 27]. Nickel has also been shown to be excellent at decomposing carbonated species, while being immune to oxidation [25, 26]. Nickel-based catalysts are, however, greatly affected by coking, which has prompted much research on new, coking-resistant catalysts. This can be done either by doping well-known nickel catalysts or by using completely different metals.

Methane steam reforming proceeds by decomposition of methane and water on the surface of the metal, with CH_4 decomposing into CH_3^*, CH_2^*, CH^*, C^* and H^* adatom compounds, and H_2O into H^*, OH^* and O^*, where * denotes a free site on the catalyst surface [25, 28–30]. These decomposition products can then recombine to form a plethora of adsorbed compounds, such as COH^*, $COOH^*$, CH_2O^*, etc. A diagram detailing this process for steam reforming (SRM), dry reforming (DRM) and partial oxidation (POM) of methane is shown in figure 2.

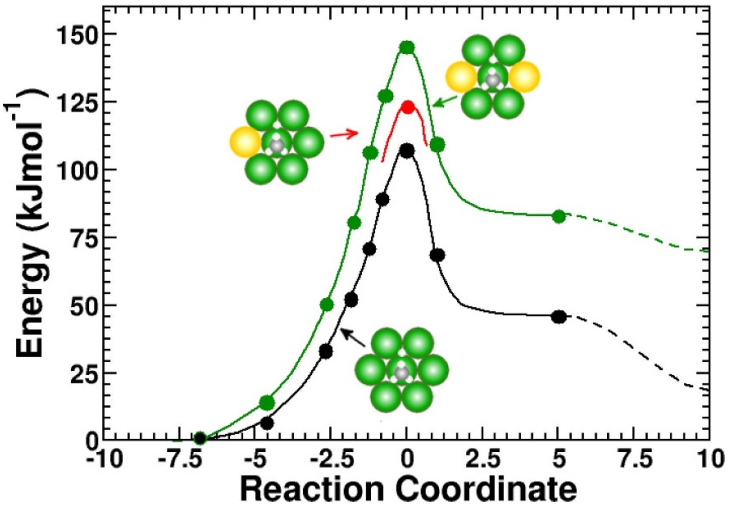

Figure 3. Energy along the reaction path of CH_4 dissociation over a Ni atom in the Ni(111) surface. Black, red and green curves present results for models of the Ni(111) surface when bare, with one and with two Au atoms, respectively. Adapted from [35], with the permission of AIP Publishing.

The presence of C* on the catalyst promotes the formation of coke. The most common strategy employed to prevent coking is to use high H_2O (steam)/CH_4 ratios [12, 31], but this generates increased costs in post-reaction separations. Thus, a lot of research has been devoted to finding catalysts that easily oxidize C* into CO [25]. Most approaches seek to compensate nickel's affinity for carbon species with oxidant elements [24, 25, 30]. Alternatively, a catalyst where C* is not prone to form, but CO is formed by dehydrogenation of COH* [29], would also be useful.

2.1.3. Multimetallic catalysts

Alloying of Ni with another metal has been considered for increasing catalyst resistance. Most nickel-based multimetallics involve alloying nickel with a noble metal, such as gold, platinum, or silver. Related TMs like copper and cobalt are also common. For the most part, the work with these multimetallics focuses on coking inhibition, while retaining or increasing activity.

Noble metals have very well-established anti-coking properties, as both monometallic [32] and multimetallic catalysts. Nearly all the work developed in this area has focused on Ni–Au catalysts, due to their high activity and strong resistance to carbon deposition. We will focus most of the rest of the section discussing Ni–Au catalysts, how research on them has evolved, and what the mechanisms underlying their properties are. As will be shown, it is not entirely clear what lies at the root of the anti-coking properties of Ni–Au catalysts.

The study of Ni–Au bimetallic catalysts for CH_4 steam reforming was kickstarted by Nørskov *et al* [33–40]. In a series of pioneering studies, feasibility and attractive anti-coking properties were established. In 1993 [33], they observed that Au atoms deposited on a Ni(110) surface, at room temperature (at which the two metals are nominally immiscible), tended to merge onto the surface layer of Ni atoms, forming a surface alloy. A later study showed that this surface alloy is only stable up to 850 K–900 K, the temperature after which the Au atoms start diffusing into the bulk [34]. A density functional theory (DFT) study [35] showed that CH_4 decomposition on the Ni(111) surface had its dissociation barrier increased by 16 kJ mol^{-1} when next to an Au atom (figure 3), which would indicate that activity is greatly diminished by the previously identified surface alloying. The authors attribute this to an energetic lowering of the local density of *d*-states on the Ni atoms in contact with Au atoms. Another study [36] determined that the presence of Au atoms on a Ni(111) surface also influences the probability of 'sticking' upon impact of a CH_4 molecule with the surface. Sticking probability decreases by ∼95% with an Au coverage as low as 0.2 monolayer (ML). This is in agreement with the results of a previous study [34], where decreased interaction with the surface upon increase in Au coverage was observed not only for CH_4, but also for CO and D_2. At Au coverages above 0.5 ML, CO and D_2 were barely adsorbed by the surface.

In a 1998 letter [37], an explicit case is made for Ni–Au industrial catalysts for steam reforming. The authors build on their previous work with a DFT study, whereby it was observed that chemisorption of carbon, C*, was much more favorable in pure Ni(111) than in Ni–Au alloys, with energy differences of up to 190 kJ mol^{-1}. It was thus possible to predict that a Ni–Au catalyst should be much less prone to graphite

formation than a pure Ni one. Experimental testing of this hypothesis was performed with a 16.5 weight % (wt%) Ni/$MgAl_2O_4$ catalyst, doped with 0.3 wt% Au. Analysis with extended x-ray absorption fine structure spectroscopy (EXAFS) showed that the Au atoms formed a surface alloy with Ni. Testing with *n*-butane steam reforming confirmed that, unlike pure Ni catalysts, the Ni–Au catalyst did not suffer from deactivation due to graphite formation. The same authors were granted a patent the next year [38], where a Ni–Au catalyst with 0.01/30% Au/Ni weight ratio, prepared by sequential impregnation, was proposed for the steam reforming of hydrocarbons 'without any carbon formation'. Once again, EXAFS showed that Au is deposited on the surface of Ni nanoparticles inside the catalyst.

In 2001, the same group [39] applied the sequential impregnation technique to create Ni–Au bimetallic catalysts, using SiO_2 and $MgAl_2O_4$ as supports. Transmission electron microscopy (TEM) and energy dispersive spectrometry (EDS) allowed the observation of bimetallic nanoparticles in both supports. However, with SiO_2, pure Au nanoparticles are also formed, separate from the bimetallic nanoparticles. Comparison of calculated x-ray absorption fine structure (XAFS) spectra and experimental EXAFS spectra for Ni–Au/SiO_2 samples shows that only ∼1/4 of the Au atoms participate in a surface alloy, with the rest forming separate pure Au phases. Monte Carlo simulations indicate that Au atoms accumulate on the edge and kink sites between low-index surface planes of the Ni nanoparticles. Thermogravimetric analysis (TGA) of $MgAl_2O_4$-supported catalysts used in the steam reforming of *n*-butane revealed that, under conditions where heavy carbon deposition occurs for the Ni catalysts, Ni–Au catalysts do not show carbon deposits.

In a highly influential theoretical study from 2002, Nørskov *et al* [40] used DFT and Monte Carlo simulations to show that carbon deposition and graphite formation tend to occur at step edges of Ni nanoparticles, and not at flat faces. They also determined that atoms from additives such as gold are more stable at precisely the same step sites, confirming the results from Monte Carlo simulations, from this and from their previous study [39]. The main function of these additives is thus blocking access to the highly reactive step sites, not in promoting oxidation of deposited carbon. This effect replicates that of H_2S, which poisons Ni catalysts in a way that prevents carbon deposition, and may be used as an additive in steam reforming processes [41, 42]. However, this also impacts catalyst activity, as step sites are also the most reactive towards CO and H_2 formation. A posterior study [43] also showed that Ni nanoparticle steps are much more active than terraces for CH_4 sticking and decomposition. Ni–Au catalysts would thus offer a compromise between improved resilience to carbon deposition and decreased activity for CH_4 decomposition. In the 2002 study [40], the authors reach the conclusion that an incomplete additive coverage would prevent graphite formation, while keeping the catalyst's activity. It is also observed that the Au atoms tend to be evenly spread on the surface of the Ni nanoparticles, not forming clusters. Similarly to what happened in their previous study [39], an EXAFS analysis of a Ni–Au/$MgAl_2O_4$ catalyst showed that Au nanoparticles are formed apart from the Ni nanoparticles. This time, 44% of Au atoms are involved in the surface alloy with Ni. These proportions seem to be related to the relative amounts of Au and Ni used during catalyst synthesis.

In 2006, in one of the first studies on Ni–Au catalyst performed by other groups, Chin *et al* [44] performed an extensive characterization of nanoparticle surface in an Au-doped Ni/$MgAl_2O_4$ catalyst. Through H_2 volumetric chemisorption, the authors were able to confirm the strong reducing effect of Au atoms on the surface of Ni nanoparticles. The presence of alloyed Au leads to decreasing chemisorption of H_2 by several times the amount of Au atoms, thus showing that their effect goes beyond site blockage. Temperature-programmed desorption (TPD) experiments with N_2O confirmed this, by showing that the presence of Au on the surface prevented the decomposition of N_2O and the formation of NiO. EXAFS tests confirmed that alloyed Au atoms have a very low coordination number, in agreement with the hypothesis that they tend to stay at the surface, away from the bulk. This work agrees with the results of previous experimental and theoretical studies performed by the Nørskov group [33, 37, 40].

Triantafyllopoulos and Neophytides [45] synthesized a Ni–Au/YSZ catalyst, with a Ni:Au ratio of 50:1, which was used to study CH_4 dissociative adsorption. The authors observed a strong inhibition of graphitic carbon formation on the surface of the catalyst, together with an increase in the activation energy for CH_4 dehydrogenation/CH_x rehydrogenation, making CH_x species more stable and easier to oxidize to CH_xO. Decreased formation of graphitic carbon is thus attributed to a decrease in C^* formation, non-inhibition of graphite formation or increased C^* oxidation.

A study by Keane *et al* [46], used the reductive deposition technique to generate an Au-doped Ni/Al_2O_3 catalyst. Energy dispersive x-ray analysis of metal nanoparticles showed that, in a catalyst with an 8.2 Ni/Au atomic ratio, surface composition was close to 1:1. This supports the observations of Nørskov *et al*, regarding the formation of surface alloys of the nominally immiscible nickel and gold.

Using Au-doped Ni/CeO_2(Gd_2O_3) as anode material in a solid oxide fuel cell, Niakolas *et al* [47] showed conclusively that the addition of Au inhibits coke formation. When performing a TGA of materials with different levels of Au, the results clearly show that the presence of Au greatly diminishes the rate of carbon

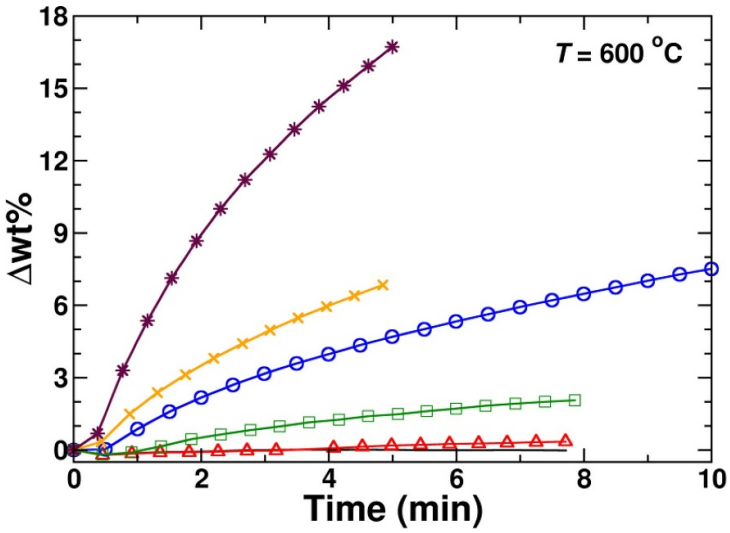

Figure 4. Thermograms for $Ni/CeO_2(Gd_2O_3)$ and $Ni–Au/CeO_2(Gd_2O_3)$ samples. Experiments performed at 600 °C, under 10 vol.% CH_4/Ar, with a total feed of 100 cc min^{-1}. The symbols represent: (*, brown) commercial $Ni/CeO_2(Gd_2O_3)$, as prepared; (×, yellow) commercial $Ni/CeO_2(Gd_2O_3)$, pre-calcined at 850 °C; (◯, blue) 1 at% $Au–Ni/CeO_2(Gd_2O_3)$, calcined at 850 °C; (□, green) 2 at% $Au–Ni/CeO_2(Gd_2O_3)$, calcined at 850 °C; (△, red) 4 at% $Au–Ni/CeO_2(Gd_2O_3)$, calcined at 850 °C; (—, black) 4 at% $Au–Ni/CeO_2(Gd_2O_3)$, calcined at 1100 °C. Adapted from [47]. Copyright (2010), with permission from Elsevier.

deposition, and increased Au content enhances this effect (figure 4). The Au was added by the deposition–precipitation method, with the presence of Au nanoparticles with tens of nanometers in diameter being confirmed by scanning electron microscopy (SEM). The existence of metallic Au in the material was confirmed by x-ray diffraction (XRD) analysis. However, it is interesting to notice that the XRD results show that metallic Au, while certainly present before the reduction step of the synthesis procedure, seems to disappear afterwards. SEM analysis also fails to find the gold nanoparticles after the reduction step, performed with 80% H_2/Ar at 800 °C, indicating that some major structural shift occurs in the material during the reduction step, making it unclear exactly what is behind the anti-coking properties of the catalyst.

Lazar *et al* [48] tested the activity of a $Ni/\gamma\text{-}Al_2O_3$ catalyst, synthesized with the co-impregnation method, by measuring CH_4 conversion in non-repeatable single runs. The authors observed a marked effect in the catalyst's performance upon the addition of noble metals. A 1%-Au/8%-Ni catalyst led to an increased activity from 40% to 60% CH_4 conversion, at 450 °C. At higher temperatures, the improvement in performance starts to disappear, and above 600 °C it shifts, with the Au-doped catalyst performing slightly worse than the original. The authors speculate that this effect may be due to alloying of the two metals, originally existing in separate nanoparticles. This hypothesis is in agreement with previous work [39, 40] suggesting Au atoms would tend to occupy the more reactive sites on the surface of Ni nanoparticles. The original catalyst was also doped with Ag, with very different results from Au doping; the Ag/Ni catalysts were almost inert, and only at 700 °C did their activity start to approach that of the other two catalysts. The authors also tested catalyst stability, by testing performance after 48 h of continuous run, at 500 °C and 700 °C. At 500 °C, Au doping strongly stabilized catalyst performance, while the original catalyst started showing signs of degradation. At 700 °C, the opposite happened, with the original catalyst having nearly identical performance, while the Au-doped one showed a slight decrease. If Au nanoparticles do exist at 500 °C, but tend to disappear at 700 °C, these results seem to indicate that coke inhibition stems from the activity of segregated nanoparticles, and not deposition on the surface of the Ni nanoparticles, with the latter actually being detrimental.

A follow-up study by the same group provided similar results [49], with some notable additional information. Exhaust gases were analyzed with a gas chromatograph, allowing them to determine the proportion of CO_2 and CO. Ni–Au catalysts strongly favor CO_2 formation, so they do not just have higher CH_4 conversion, but also higher H_2 production, through the WGSR. The authors were also able to determine, through TGA of used catalysts, that Ni–Au and Ni–Ag catalysts are not only far less susceptible to carbon deposition, but the kind of carbon that is deposited is different. Standard deactivation from carbon deposition involves the formation of graphitic crystallites, which the presence of Au and Ag hinders, with the small amount of carbon deposited being amorphous. However, these catalysts were still subject to degradation, at high temperatures, which the authors attributed to site blockage on the surface of Ni nanoparticles, induced by the formation of a surface alloy from initially segregated nanoparticles.

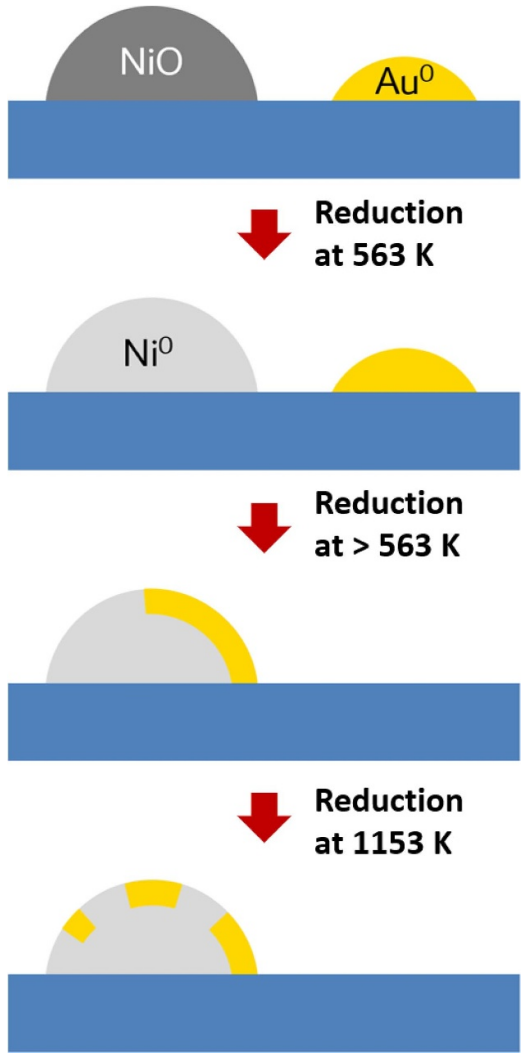

Figure 5. Alloying effect of temperature on Ni–Au catalysts. Adapted from [18]. CC BY 4.0.

The idea that Ni–Au alloys are only formed in solid-supported catalysts at high temperatures is reinforced by a characterization study conducted by Maniecki *et al* [50], where x-ray photoelectron spectroscopy (XPS) and XRD spectra indicate that Au and Ni co-exist as an alloy on the surface of the catalyst only after it is exposed to high temperatures.

In their review of 2013, Wu *et al* [18], taking a lead from the work of Maniecki [50] and Lazar [48, 49], conceived of a mechanism for the formation of Ni–Au alloys in bimetallic catalysts prepared by the co-impregnation method, whereby effective reduction of NiO and temperature are the decisive factors determining the extent and kind of alloying that takes place, where, originally, the two metals were segregated in separated nanoparticles. This view is well represented in the scheme in figure 5. This alloying effect, induced by reduction and high temperatures, would neatly explain the 'disappearance' of gold nanoparticles in the work of Niakolas *et al* [47], occurring precisely after a reduction step at high temperatures. Interestingly, the suggested cut-off temperature for the formation of the alloy, 1153 K, is remarkably close to the critical point of the miscibility gap of 1089.5 K reported by Wang *et al* [51]. However, this temperature is also similar to those used in post impregnation calcination and reduction [39, 44–46, 48], so studies suggesting both the surface alloy and the segregated Au nanoparticles perspective employ the kind of temperatures Wu *et al* suggest give rise to the alloying effect.

Focusing again on the supposed activity of step sites, Arevalo *et al* [29] investigated the reasons behind the strong binding of C^* on Ni nanoparticle step sites, by using dispersion-corrected DFT-based first principles calculations. Comparing the interaction energy of the several decomposition fragments of CH_4 on Ni and Ru steps, the authors determined that $C^* + 4H^*$ is the most favored species for Ni, but not for Ru, which rather favors $CH^* + 3H^*$. Their explanation for this is that C^* at Ni steps can interact with five Ni atoms, four at the surface and one beneath the surface, while with Ru it interacts only with four surface atoms. In the case of Ni, when the subsurface atom is replaced for an Au atom, the C^* interaction is greatly

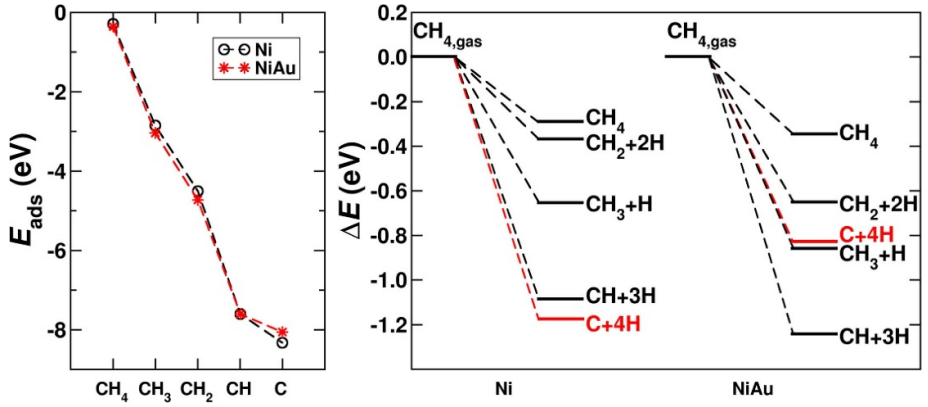

Figure 6. Adsorption energy of CH_x (left) and reaction energies for CH_4 dissociation into $CH_y + zH$ ($y + z = 4$) species (right) on stepped Ni and Ni–Au systems. Adapted with permission from Springer Nature Customer Service Centre GmbH: Springer Nature, Scientific Reports [29] © 2017.

decreased, and $CH^* + 3H^*$ is once again the most stable state (figure 6). However, it is unclear how this could explain the anti-coking effect of Au, as the authors do not present any mechanism for the formation of the 4Ni + 1Au configuration on the step sites of Ni nanoparticles. Indeed, many other authors [33, 37, 40, 44] have shown that the Ni–Au alloy formed tends to be concentrated on the surface, with only high temperatures allowing Au diffusion into the bulk [44].

Following the Ni nanoparticle modification perspective, de Oliveira Rocha *et al* [52] performed an in-depth study of surface modification of a Ni/Al_2O_3 catalyst through sequential impregnation with Au. By using diffuse reflectance infrared Fourier transform spectroscopy (DRIFTS) of adsorbed CO, the authors were able to study the changes that Au impregnation induced on the surface of Ni nanoparticles in the catalyst. Among many subtle changes, it was possible to ascertain the preferential alloying of Au atoms on Ni atoms with low coordination (i.e. steps, corners, and surface irregularities). However, there would still occur some Au deposition on Ni(111) atoms, which increases local electron density, thus promoting a preferential adsorption of CO in the linear form (with faster kinetics), instead of bridge form. Testing of the catalyst in a fixed bed reactor showed that the apparent activation energy of the steam reforming reaction was greatly affected by Au impregnation, which is attributed to a decrease in available low coordination Ni atoms. The authors thus point to two factors underlying the decreased carbon deposition in Au-doped Ni catalysts; deposition in low coordination sites hinders CH_4 decomposition, and deposition in high coordination sites promotes faster CO desorption. At low temperatures, CO formation is typically the rate determining step (rds) [26], so Au deposition has the effect of 'the steps of methane activation and carbon oxidation becoming equilibrated.'

While it is entirely certain that Au atoms are sometimes deposited on top of Ni nanoparticles forming a surface alloy [39, 40, 44, 52], and that on other occasions segregated Au nanoparticles have been detected [47–49], it is frequently impossible to ascertain whether both forms co-exist in the same material. The study by Molenbroek *et al* [39] is perhaps the only one that, by employing TEM/EDS, comes close to excluding the formation of independent nanoparticles. Still, it seems to us that the mechanisms and conditions behind the formation of segregated Au and Ni nanoparticles, a surface alloy, or both, has yet to be unveiled. Furthermore, the way segregated Au nanoparticles are able to condition the formation of graphitic carbon remains a mystery. It is possible that the studies where formation of segregated nanoparticles was detected failed to detect the additional formation of Ni nanoparticles with a Ni–Au surface alloy, which would function in the way Nørskov *et al* have discovered. Without further studies on this issue, we believe this should be the default hypothesis.

Xu *et al* [53] developed a computational approach to screen the potential of a large number of TM alloys for the reaction of SRM by separately performing microkinetic modeling of all the elementary reactions involved, employing energies of reaction intermediates and transition states from scaling relations using the binding energies of carbon and oxygen as descriptors. After having established a volcano-shaped relationship for the reaction as a function of the two descriptors above, they were able to predict the rates under *operando* conditions of binary alloys based on the A_3B or AB (A and B are TMs) stoichiometries, with stability close to the stabilities of the bulk pure A and B metals and stability against oxidation. They found that A_3B-like alloys derived from the cheap Ni, Fe and Co elements were very active and stable. Importantly, Ni_3Fe and Co_3Ni alloys displayed activity either with AA or AB terminations. Encouragingly, NiFe and NiCo alloys were

experimentally found to display interesting activities for the reaction. However, it seems that the exact composition of the catalyst has a decisive role, and alloying, by itself, is not a solution. In fact, the effect of Fe on NiFe catalysts has been found to have both positive and negative influence in the catalytic activity in the reforming of hydrocarbons [54]. On the one hand, the activation and dissociation of C–H and C–C bonds occur mostly on surface Ni atoms. Thus, the alloying with Fe will lead to a decrease in the number of the most active sites. On the other hand, Fe is oxidized more easily than Ni and the iron oxide formation was associated to suppressing of carbon deposition and assistance in reactions between carbonaceous with oxide species. Therefore, while computational studies are certainly relevant for fast screening of materials, further experimental optimization of catalysts under *operando* conditions is needed.

2.2. Water–gas shift reaction

2.2.1. Introduction

The term water gas stands for an equimolar mixture of carbon monoxide and hydrogen that is produced by passing steam over heated coke, following the general reaction:

$$C + H_2O \rightarrow CO + H_2\,,\ \Delta H = 131\ \text{kJ mol}^{-1} \tag{4}$$

In the 19th century, the reaction described by equation (4) was employed, for example, to enrich the gas generated for residential and commercial use in heating and lighting. More recently, as pointed out above, the production of steam gas is based on the SRM:

$$CH_4 + H_2O \rightarrow CO + 3H_2\,,\ \Delta H = 206\ \text{kJ mol}^{-1} \tag{5}$$

providing a high molar ratio of H_2 over CO. In both cases, the aim is to obtain hydrogen-rich streams for numerous applications, namely, as a reactant in fuel cells or in the ammonia synthesis (see below). The WGSR, equation (2), discovered by Felice Fontana in 1780 [55], is a reversible chemical reaction between carbon monoxide and steam to produce carbon dioxide and hydrogen.

The WGSR has been carried out in industry in two steps using two different temperatures. This is because the reaction is exothermic, hence favoring formation of products at low temperatures, but its kinetics is very slow. Hence, a step at high temperature (high-temperature shift, HTS) is employed to reach the equilibrium faster, and then a step at a lower temperature (low-temperature shift, LTS) is used to achieve almost full conversion of CO. The HTS uses a catalyst based on iron oxide (chromium oxide has been also employed for catalyst stabilization and copper or other supported metals may be present) that works at temperatures well above 300 °C (the catalyst is inactive below this temperature). The reaction mixture from the HTS is then cooled to ∼200 °C in the LTS reactor, which employs catalysts based on copper (conventionally, $Cu/ZnO/Al_2O_3$) which become inactive above 250 °C. In the HTS step, the content of CO in the feed stream is usually reduced to 2% and in the LTS step it is reduced to <0.5%. In fact, from the equilibrium constant as a function of the temperature [55],

$$K = e^{\left(\frac{4577.8}{T} - 4.33\right)}. \tag{6}$$

It is clear that the equilibrium CO content is 20 times lower at 200 °C than at 400 °C. Because the total number of moles is the same in the reactants and in the products, pressure cannot be employed to force the conversion towards the desired products but is often employed to increase the reaction rate, hence allowing the equilibrium to be attained faster. Cryogenic, membrane, separation with solvents or sorbents are common strategies used for separating CO_2 from gas mixtures. Due to its high energy efficiency and because CO_2 interacts much stronger with most adsorbents than H_2, pressure swing adsorption is the method of choice for separating carbon dioxide from hydrogen, leading to hydrogen purities over 99.9%.

While the catalysts above have been used for several decades, they suffer from several shortcomings. For example, although catalysts based on Fe/Cr oxides are stable against sulfur poisoning, that is only the case if the amounts of sulfur are small. Also, if metallic iron species are present in the Fe/Cr catalyst, methanation of carbon monoxide via:

$$CO + 3H_2 \rightarrow CH_4 + H_2O\,,\ \Delta H = -206\ \text{kJ mol}^{-1} \tag{7}$$

takes place, leading to hydrogen consumption. The presence of Cr(VI) in the HTS catalysts is also a problem because this ion is carcinogenic to humans. Similarly, Cu-based catalysts are sulfur-sensitive and Cu crystallites are prone to thermal sintering. Thus, strong effort is being made to find catalysts with improved characteristics for the WGSR. Apart from being active for the WGSR, the required catalyst must have thermal and air stability for long term activity, and has to be cheap. Therefore, obvious choices are catalysts mainly

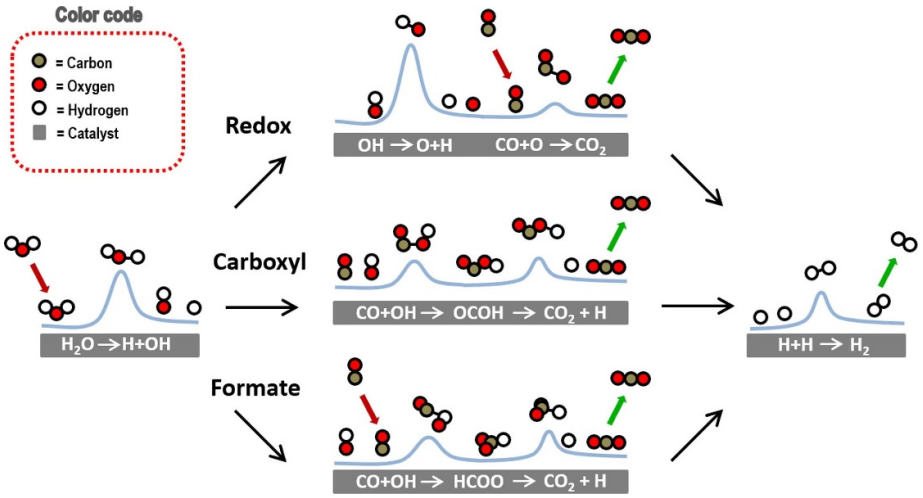

Figure 7. Schematic representation of the three accepted mechanisms for the WGSR. Red and green arrows are used for adsorption of reactants and desorption of the reaction products, respectively. Blue lines approximate the barrier heights of the different elementary reactions. Adapted from [57], Copyright (2018), with permission from Elsevier.

constituted by cheap metals or metal oxides incorporating highly dispersed/diluted (expensive) metals. Potential elements for catalytic applications are the abundant Cu, Fe, Zn, Al or Cr, which are already found in the industrial WGSR catalysts, and Co or Ni. While metallic copper is the most active pure metal catalyst [56], it might be possible to obtain improved catalysts by mixing elements (or more complex materials) that display distinct characteristics, i.e. stronger or weaker adsorptions of WGSR reactants, intermediates and products than those found for metallic copper, until reaching an optimal balance, i.e. the top of the volcano.

It is generally accepted that the WGSR proceeds through one of the following reaction routes, viz. the (a) redox, (b) formate or (c) carboxyl mechanisms (figure 7). The redox pathway is characterized by the complete dehydrogenation of water on the catalyst surface, while the associative formate and carboxylic routes are named so because they lead to the formation of these intermediate species upon the reaction of carbon monoxide with surface hydroxyl species.

Importantly, the first step of the WGSR, i.e. the dissociation of water into H and OH adsorbed species (figure 7), was found to be the rate determining one on Cu and on Au surfaces or nanoparticles [58–60]. It was predicted from DFT calculations for the WGSR on planar and stepped copper surfaces that the associative mechanism through the carboxyl intermediate, where carboxyl dehydrogenation is assisted by co-adsorbed hydroxyl species, is energetically more favorable.

2.2.2. Monometallic catalysts

The role of the different components of the industrial WGSR catalyst is not clear but the availability of metallic Cu species seems to be important, both in the LTS and in the HTS catalysts. For example, Yahiro *et al* [61] used the conventional impregnation method to prepare several catalysts based on Cu–ZnO supported on oxides with high surface area, namely, Al_2O_3, MgO, SiO_2–Al_2O_3, SiO_2–MgO, β-zeolite and CeO_2, and found that the reducibility of CuO is an important factor controlling the activity of the catalyst with the best activities found when JRC-ALO-8 alumina was employed as the support, followed by JRC-ALO-5 alumina and CeO_2. Interestingly, the addition of CuO to the HTS Fe_3O_4/Cr_2O_3 catalyst promotes the reaction but with contradictory views. Rhodes and Hutchings [62] proposed that metallic Cu is not present and that the catalytic improvements are caused by Cu^{2+} species acting in solid solution, which modify the electronic properties of the Fe_3O_4/Cr_2O_3 catalyst and lead to a significant decrease in the activation energy from 118 to 75–80 kJ mol^{-1}. However, Puig-Molina *et al* [63] performed *in-situ* XAFS studies of a Cu-promoted Cr-stabilized iron oxide catalyst at 380 °C and elevated pressures and concluded that metallic Cu forms at 250 °C, promoting the WGSR activity that is due to the magnetite surface incorporating Cr^{3+} species. The formation of metallic Cu species at temperatures above 250 °C was confirmed by Estrella *et al* [64] from *in-situ* time-resolved XRD, XAFS, and atomic pair distribution function analysis of the behavior of $CuFe_2O_4$ and Cu/Fe_2O_3 catalysts under WGSR conditions. More recently, Zhang *et al* [65] carried out a comprehensive experimental and computational study with the aim of identifying the WGSR active sites on copper-based catalysts. These authors developed an experimental strategy to synthesize uniform cubes, octahedra and rhombic dodecahedra Cu nanocrystals, with well-defined {100}, {111}, and {110} surfaces and size distributions of 1000 ± 150, 1056 ± 207, and 595 ± 113 nm, respectively, from the corresponding Cu_2O

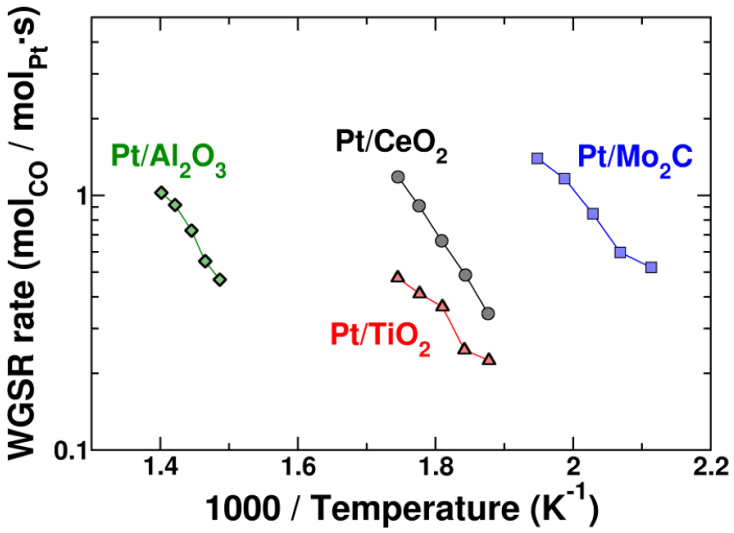

Figure 8. Arrhenius plots of the WGSR rates for 2.7% Pt/Al_2O_3, 5% Pt/CeO_2, 2% Pt/TiO_2, and 4% Pt/Mo_2C catalysts. Adapted with permission from [67]. Copyright (2011) American Chemical Society.

nanocrystals. They then found the cube/octahedron to be the most/least active which was attributed to a higher {100}/{111} facets ratio in the former than in the latter. Moreover, the experimental findings suggest that all the elementary surface reactions occur at the Cu–Cu suboxide interface of the Cu(100) surface. Separate DFT calculations employing Cu(100) and Cu(111) surfaces, bare or with Cu_2O islands to model the Cu/Cu oxide interface, confirmed that the reactions were in general more facile on the Cu(100) model with Cu_2O islands, with reactants, intermediates and products of the WGSR adsorbing on the metallic atoms in the vicinity of Cu_2O [65]. The oxygens of the oxide assume an important role in interacting with and then adsorbing the hydrogen atom originating from the water dissociation, the rds on metal surfaces [58–60]. In fact, when the reaction takes place at the Cu/Cu oxide interface, the energy barrier is 0.4 eV, significantly smaller than the value (1.2 eV) calculated on Cu(100) and on several other surfaces [66].

Schweitzer *et al* [67] compared the role of different supports, namely, non-reducible Al_2O_3, reducible CeO_2 and TiO_2, and Mo_2C, in the catalysis of the WGSR by platinum. Notably, as can be seen in figure 8, the Pt/Al_2O_3 catalyst is clearly less active than those using cerium or titanium oxides supports, and the three oxides are less interesting than the molybdenum carbide support.

The increased activity of platinum catalysts when supported on reducible oxides than on non-reducible ones was observed in other studies. For example, Phatak *et al* [68] compared the WGSR on Pt catalysts supported on ceria and alumina, at $p = 1$ atm, $T = 180$ °C–345 °C, and found that the turnover frequency (TOF) was 30 times higher on ceria-supported Pt than on the corresponding alumina-supported catalysts. Results in the same direction were obtained by Panagiotopoulou and Kondarides [69] upon comparison of several reducible, namely, TiO_2, CeO_2, La_2O_3, and YSZ, and non-reducible, namely, Al_2O_3, MgO, and SiO_2, metal oxides. In particular, the latter authors found that the TOF of CO conversion did not depend on metal loading, dispersion or crystallite size, but depended strongly on the nature of the metal oxide carrier, with the catalytic activity being 1–2 orders of magnitude higher when the active metal (e.g. Pt or Ru) is supported on reducible oxides [69]. In brief, the easier extraction of oxygen from reducible oxides increases the activity of the reaction since this facilitates the oxidation of CO molecules adsorbed on the supported metal. The support is then oxidized by oxygen originating from water. Therefore, in such situations, not only the supported metal but also the partially reduced metal from the oxide actively participated in the reaction, thus resembling a multimetallic catalyst as those reviewed below.

2.2.3. Multimetallic catalysts based on copper

As stated in the previous sub-section, subtle changes in the nature of the different species in the catalyst may lead to important improvements in the catalysis of the WGSR. Therefore, significant efforts were made to analyze the influence of a second metal in the catalysis of this reaction.

WGSR catalysts based on monometallic (Ni and Cu) and bimetallic (Ni–Cu, 1:1 alloy confirmed by x-ray absorption spectroscopy, XAS) particles anchored on SiO_2 were synthesized via an *in-situ* self-assembly core–shell precursor route by Ang *et al* [70]. The CO conversion measured at 400 °C for catalysts with a total of 10% metal loading, prepared with a small amount of oleic acid (OA) to aid metal dispersion, was 97% in the case of the bimetallic $5Ni5Cu/SiO_2$ catalyst, 92% in the case of $10Ni/SiO_2$ and 84% in the case of

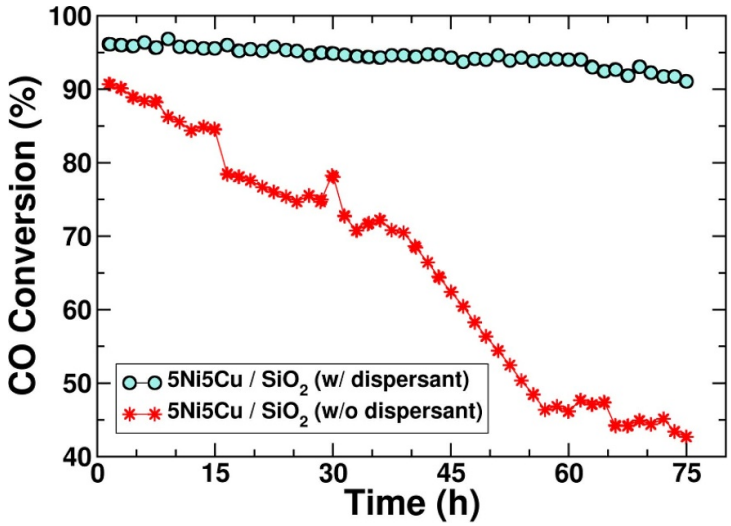

Figure 9. CO conversion to CO_2 for 75 h reaction with 5Ni5Cu/SiO_2 catalysts prepared with (cyan) or without (red) the oleic acid (OA) dispersant. Adapted from [70] with permission of The Royal Society of Chemistry.

10Cu/SiO_2, but at lower temperatures, e.g. 250 °C, only monometallic copper catalysts could convert CO. Lower conversions were obtained for catalysts prepared without the addition of the dispersant, suggesting that smaller particle sizes enhance WGSR activity. Moreover, as can be seen in figure 9 for the bimetallic 5Ni5Cu/SiO_2 catalyst, while the CO conversion of the sample prepared with OA remained stable for a runtime of 75 h, the CO conversion is halved in the case of the catalyst prepared without the dispersant, which suggests less stable metal-support interactions with subsequent metal sintering in the latter.

Catalysts prepared with/without the dispersant displayed H_2 yields of 50%/45% but the monometallic nickel catalysts were not selective and led to formation of small amounts of methane. The observations were then rationalized by Ang *et al* upon analysis of *in-situ* DRIFTS results collected at different temperatures and CO-temperature-programmed-reduction-mass spectroscopy data. In the catalysts containing Cu, CO adsorption occurs at Cu sites which are known to be less active than Ni sites for CO cleavage, hence avoiding the formation of carbon precursors that are eventually hydrogenated to methane. Also, Ni segregation is suppressed in the bimetallic catalysts, otherwise, methane would form as in the 10Ni/SiO_2. The formation of smaller metal clusters when OA is employed in the catalyst preparation enhances metal-support interactions, hence increasing the catalyst stability. Also, XAS results suggest that NiO species occurring at the bimetallic particle-support interface remain unreduced even at 450 °C, conferring increased stability because of the formation of stronger particle-support interactions. Concomitantly, the CO adsorption is stronger than in the case of large particles and the CO surface species become closer to hydroxyl groups on the SiO_2 support, clearly suggesting a synergic behavior in the multimetallic catalyst.

Qualitatively similar results were found by Saw *et al* [71] for Ni/Cu catalysts supported on ceria, upon variation of the molar ratio of copper and nickel from 0 to 1 with 10 wt% loadings of their metal nitrates; the catalysts obtained were denoted 10Ni, 9Ni1Cu, 5Ni5Cu, 1Ni9Cu and 10Cu. The 5Ni5Cu/CeO_2 catalyst was found to exhibit the highest reaction rate with the least methane formation, which was attributed to the formation of a Ni–Cu alloy phase and the stabilization of the CO adsorbed species. Kinetic studies revealed that one-site carboxyl mechanism could be the main reaction pathway with formate acting as spectator. However, other possibilities, e.g. combination of both carboxyl/redox and formate/redox routes could not be ruled out.

Arbeláez *et al* [72] investigated the WGSR over structured Cu, Ni, and bimetallic Cu–Ni supported on activated carbon catalysts. Two bimetallic catalysts with fixed Cu:Ni molar ratios of 2:1 and 1:2 were prepared. Again, the results pointed out to the formation of a Cu/Ni alloy with Cu having the important role of mitigating the methanation activity of Ni by controlling the CO adsorption behavior and dissociation ability as suggested by Saw *et al* [71], consequently favoring the shift process. Interestingly, CO conversion was found to be the highest in the case of the Cu-rich bimetallic catalyst with activity comparable to those demonstrated by catalysts based on noble metals deposited on ceria. The higher activity of Cu-rich bimetallic catalysts towards the WGSR was also reported by Jha *et al* [73] who studied mesoporous NiCu/CeO_2 catalysts with weight percentage ratios of Ni/Cu from (1:1) to (1:4). Importantly, while metallic phases of Cu and Ni were observed in the XRD patterns of Cu/CeO_2 and Ni/CeO_2, respectively, after being tested in the WGSR at temperatures up to 550 °C, in the case of the reduced NiCu(1:4)/CeO_2 catalyst only the metallic phase of

copper was found, which was interpreted as a result of Cu segregation to the surface layer, a point of view that is supported by the results of Lin *et al* [74].

More recently, Pastor-Pérez *et al* [75] revealed that bimetallic NiCu formulations are not always advantageous for the WGSR. In fact, for catalysts prepared on a CeO_2/Al_2O_3 support, the monometallic Cu catalyst was more active in both model and post-reforming WGSR mixtures at low-medium temperatures than the bimetallic CuNi systems. Only for medium–high temperatures does the bimetallic CuNi(1:1) outperform the stability levels reached with the monometallic formulation, becoming an interesting choice even when start-up/shutdowns operations are considered during the catalytic experiments. These observations agree with those of Ang *et al* [70] presented above but using a SiO_2 substrate. Computational studies were also performed to obtain a detailed structural and energetical understanding of the WGSR. Liu *et al* [76] performed DFT calculations, with the Perdew–Burke–Ernzerhof (PBE) functional and Gaussian-type orbitals, for the WGSR occurring on $TM_1@Cu_{12}$ particles, with TM = Co, Rh, Ir, Ni, Pd, Pt, Cu, Ag, and Au, i.e. with the TM atom at the center of the particle, surrounded by 12 copper atoms. They found that the reactions proceed through the carboxyl mechanism, while the redox and formate routes arise as minor channels in the WGSR on the Cu-based particles, a finding that agrees with calculated data on extended pure-Cu surfaces [59]. On the $TM_1@Cu_{12}$ particles, the formation of carboxyl species (COOH) from co-adsorbed CO and OH was found to be the rds when TM = Ag, while the dissociation of the carboxyl species into co-adsorbed CO_2 and H species is the rds for TM = Co, Ni, Rh, Pd, Ir, and Au, and the formation of co-adsorbed CO_2 and H_2 from CO_2 and H species is the rds for TM = Cu and Pt. These authors combined the energetic span model of Kozuch and Shaik [77] with the calculated free energy profiles to find the turnover-determining transition state (TDTS) and the turnover-determining intermediate (TDI) which govern TOF and selectivity. Interestingly, upon the consideration of the energetic span model, the TDTS and the TDI are the same for all systems, respectively, the transition state corresponding to the formation of carboxyl species (COOH) from co-adsorbed CO and OH and the state for co-adsorbed CO, H and OH species. The highest TOF was calculated for the $Co_1@Cu_{12}$ cluster, with the group 9 elements, Co, Rh, and Ir, having TOFs that are higher than those for TM from groups 10 or 11, hence, more promising catalyst candidates for the WGSR.

Luo *et al* [78] investigated the WGSR on $PdCu/CeO_2$ also by means of DFT calculations, employing the PBE approach with D3 dispersion corrections and plane-wave basis sets. The calculations considered an unsupported $PdCu_3(111)$ slab and a PdCu particle, with eight Pd and 12 Cu atoms per unit cell, that was deposited on a slab of CeO_2. In the case of the unsupported $PdCu_3(111)$ slab, water was found to adsorb very weakly ($E_{ads} = -0.05$ eV, the negative value meaning favorable adsorption) while the barrier for its dissociation was quite large ($E_{act} = 1.42$ eV), which suggests that water dissociation is difficult, as confirmed by microkinetic simulations to be the rds. The water dissociation barrier on the $PdCu/CeO_2$ interface is significantly reduced to $E_{act} = 0.24$ eV, suggesting a more active catalyst for dissociating water, but where the dissociation of the hydroxyl species is slow. The calculations also show that CO adsorption is stronger on Pd than on Cu, which suggests that Pd plays a key role in the WGSR by capturing CO molecules from the gas-phase.

Saqlain *et al* [79] studied the WGSR on metallic Cu(100) and bimetallic Cu–Au(100) surfaces with a DFT approach (Perdew–Wang 91 (PW91) functional) and plane-wave basis sets. The results of their calculations predicted that the bimetallic surface is superior to the Cu(100) surface for the catalysis of the WGSR, since the decomposition of water, which is difficult on the metallic surface, becomes energetically more favorable on the bimetallic surface. The charge transfer from the exposed Cu layer to the underneath Au layer was suggested to be the main reason for the enhanced activity, with CO oxidation following the redox path on both the surfaces. On the bimetallic surface, the rds was linked to the O–H disproportionation reaction leading to O and H_2O.

The computational studies above clearly suggest that active WGSR catalysts must be able to easily dissociate the water molecule. Therefore, several researchers focused their attention on the reaction of water dissociation on targeted catalyst models instead of calculating the full WGSR mechanism. Ghosh *et al* [80] used the PBE functional and plane-wave basis sets to study the water adsorption and dissociation on Cu/Ni bimetallic surfaces with varying concentration of the two metals. Overall, their calculations show that the presence of Ni in Cu(111) surfaces decreases the activation energy barriers for water dissociation, with values decreasing from 1.14 eV on Cu(111) to 0.61 eV in the case of a Ni monolayer on top of Cu(111), but the adsorption energies are almost constant with values between −0.12 and −0.18 eV. In absolute value, the activation energies are larger than the adsorption energies, suggesting that water molecules will desorb intact without dissociating upon temperature increase.

Bimetallic catalyst models based on Cu(110) and Cu(111) surfaces, with one outermost Cu atom replaced by Ni, Rh, Ir or Ag, were considered in another DFT study by Fajín *et al* [81] performed with the PW91 functional and plane-waves. The selection of the dopant elements was based on previous studies by

Table 1. CO uptake, CO_2 production rate and TOF of WGSR catalysts working with a 10% CO and 20% H_2O stream at 543 K. Reprinted from [98]. Copyright (2018), with permission from Elsevier.

Catalyst	CO uptake/μmol g^{-1}	CO_2 rate/μmol min^{-1} g_{Pt}^{-1}	TOF/10^{-3} s^{-1}
Fe/SiO_2	—	0	0
Pt/SiO_2	49	659	10.4
Physical mixture (Fe/SiO_2 + Pt/SiO_2)	—	511	7.2
$Pt_1Fe_{0.06}/SiO_2$	32	590	15.3
$Pt_1Fe_{0.1}/SiO_2$	30	839	25.8
$Pt_1Fe_{0.16}/SiO_2$	29	1503	48.9
$Pt_1Fe_{0.2}/SiO_2$	27	1525	47.5
Pt/C	95	0	0
$Pt_1Fe_{0.2}/C$	76	89	1.5

the same authors [82] that suggested surfaces of Ni, Rh, Ir and Ag to be quite interesting for dissociating a water molecule. Upon comparison of the adsorption energies and of the activation energy barriers on the bimetallic surfaces with those calculated on parent metallic surfaces, these authors found a cooperative effect (i.e. more pronounced effect in the bimetallic surfaces than in the corresponding parent pure metallic surfaces) that stabilizes the reactants and products of the water dissociation reaction and leads to a decrease of the energy barriers associated to the cleavage of the O–H bond in the water molecule. Importantly, the absolute values of the adsorption energies for the water molecule become larger than the activation energy barriers on the bimetallic surfaces, suggesting that the water molecule will effectively dissociate into co-adsorbed H and OH species, with Rh@Cu(110) and Ir@Cu(110) being very interesting cases with adsorption energies/activation energy barriers of −0.51/0.31 eV and −0.55/0.21 eV, respectively. Fajín *et al* [83] extended their computational studies to trimetallic catalyst models and found that the replacement of two outermost atoms by one Al and one Zn atom in extended copper surfaces dramatically improves the activity of the copper surface towards the dissociation of the water molecule. Among the 25 trimetallic catalyst models considered in their work [83], the calculations predict a facile dissociation of the water molecule onto the (AlZn)@Cu(111) surface, which is aligned with the experimental results by Boumaza *et al* [84] where the potential of a $Cu_{0.5}Zn_{0.5}Al_2O_4$ spinel oxide catalyst for the WGSR was demonstrated. The high activity of the ternary Cu/Zn/Al catalyst suggests that the active phase of the $Cu/ZnO/Al_2O_3$ commercial catalyst might embody localized patches of a trimetallic alloy containing these metal atoms [85]. A spinel phase but with Fe instead of Al ($Cu_{0.15}ZnFe_2$) was also found to be quite active for the WGSR [86]. In fact, the trimetallic catalyst was found to be more active than bimetallic Cu–Zn and Cu–Fe oxide catalysts which was suggested to be a consequence of the lower temperature required for reducing CuO in the spinel catalyst than in the bimetallic oxides [86], which is well aligned with the suggestions by Yahiro *et al* [61] discussed above. However, in the works by Khan *et al* [87] and Natesakhawat *et al* [88], where several different $Fe_{2.73}M_{0.27}O_4$ (M = Al, Ce, Co, Cr, Cu, Ga, Mn, Ni and Zn)-type spinels were studied, the complexity of the process became evident, since different aspects, e.g. improved covalency of the $Fe^{III} \leftrightarrow Fe^{II}$ redox couple, sintering restriction, decrease of the temperature for $Fe_2O_3 \rightarrow Fe_3O_4$ reduction, or mobility of lattice oxygen, may be differently influenced by the added metal.

2.2.4. Multimetallic catalysts based on platinum

Platinum particles dispersed over metal oxide supports such as Al_2O_3, CeO_2, ZrO_2, CeO_2–ZrO_2, or TiO_2 display interesting activity for the WGSR at low temperatures [68, 89–97]. Therefore, it is not surprising to find studies where the effect of the addition of a second metal in the catalytic activity towards the WGSR was analyzed. For example, Aragao *et al* [98] used the method of controlled surface reactions (CSRs) to incorporate Fe into Pt/SiO_2 with 5 wt% Pt loading, with Pt to Fe molar ratios between 1:0.05 and 1:0.2. The deposition of Fe was suggested to occur near uncoordinated atoms at the edges and corners of the Pt nanoparticles and/or activated hydroxyl groups at the interface with the support. Notably, no Fe deposition could be detected on the bare SiO_2 support, clearly suggesting that OH groups on the bare support were not having the same characteristics as those in Pt/SiO_2. The catalytic activities of the bimetallic $FePt/SiO_2$ catalysts are compared with those of the monometallic catalysts, bare and physically mixed, in table 1. The influence of the support was also analyzed upon additional comparison with carbon supported Pt/C and $Pt_1Fe_{0.2}/C$ catalysts.

As can be seen, when Fe is added to the Pt-based catalysts, the CO uptake decreases but the CO_2 production rates increase, clearly showing the synergic influence of iron in the WGSR catalysis. Also, the comparison of results for similar catalysts but with silica or carbon supports clearly suggests the participation of the hydroxyl groups on the silica surface in the catalysis of the WGSR. Aragao *et al* suggested that in the case of the monometallic Pt/SiO_2 and Pt/C catalysts, the reaction follows the associative mechanism, i.e. a

Langmuir–Hinshelwood type process where the adsorbed CO reacts with surface OH, generated by H_2O activation, and progressing through carbonate/carboxyl or formate intermediates. In the case of the iron containing catalysts, the Fe promoting role was explained in terms of the redox properties of Fe, where coordinatively unsaturated ferrous sites confined near the Pt–SiO_2 interface decrease the energy barriers for O_2 activation and reaction with CO adsorbed on a nearby Pt site. Nevertheless, an associative mechanism in which the coordinatively unsaturated ferrous sites are highly active for H_2O activation and dissociation could not be disregarded.

The CSR method was also used by Sener *et al* [99] to prepare MoPt bimetallic catalysts on carbon and silica supports. As in the case of the FePt bimetallic catalysts, the catalytic activities of silica-supported catalysts are higher than the ones displayed by the carbon-supported samples. Interestingly, they found that the deposition of Mo onto Pt/C reaches saturation for a composition of Mo:Pt = 0.32 and, beyond this point, the additional Mo species are deposited on the carbon support. Moreover, the TOFs on the PtMo/C catalysts were found to scale linearly with the estimates of surface Mo mole fraction, which suggests that surface Pt–Mo interfaces are the active sites for the WGSR.

Rhenium was found to enhance the activity and stability of Pt-based catalysts, even at very low temperatures [100–102]. The experimental study of Duke *et al* [103] aimed to understand the origins of the activity enhancement when compared with monometallic Pt-supported catalyst, by controlling the effects of Re oxidation and bimetallic composition, and confirming the absence of cluster sintering during reaction. Bimetallic catalysts having a large fraction of surface Pt atoms were found to be more active than bimetallic catalysts having a large fraction of surface Re atoms, which was suggested to be a consequence of the lower activity of Re towards the WGSR. However, the lower activity of Re does not explain why bimetallic catalysts with large fractions of surface Pt atoms are also more active than pure Pt catalysts. Duke *et al* [103] confirmed that only metallic Re is present in the case of the more active catalysts with large fractions of surface Pt atoms and that when ReO_x species were present the catalytic activity was reduced. From infrared absorption reflection spectroscopy experiments on pure Pt and Pt–Re surfaces, they found that the CO coverage is greater on Pt. This information was used to propose that Re species avoid catalyst poisoning by CO, as found by others [104–106], thus enhancing the catalytic activity. DFT calculations also demonstrate that CO binds more strongly to Pt than to Pt–Re. In particular, the study by Detwiler *et al* [107] confirmed previous evidence that Re is inserted within the Pt layers, leading to the formation of a Pt skin instead of the formation of a ReO_x layer. The presence of subsurface Re species lowers the d-band center of the exposed Pt atoms which results in weaker adsorbate binding.

2.3. Methanol decomposition

2.3.1. Introduction

Methanol (CH_3OH) contains 13 wt% of hydrogen [108] and is a potential hydrogen carrier (from the capture of CO_2 and from water splitting H_2) as comprehensively documented by Frei *et al* [109]. Its decomposition for hydrogen production can be represented as follows,

$$CH_3OH \rightarrow CO + 2H_2 \tag{8}$$

i.e. each mole of methanol decomposes into two moles of hydrogen. This reaction is endothermic, with $\Delta H = +91.7$ kJ mol^{-1} (around 1 eV) at 298 K [12]. The resulting CO may be combined with steam to produce additional H_2 via the WGSR equation (2). One of the difficulties of using methanol to produce hydrogen to fuel the engine of a vehicle are the high temperatures required, a problem which affects especially Northern countries. In fact, while the methanol synthesis requires low temperatures and high pressures, its decomposition is performed at ambient pressure and higher temperatures [110].

2.3.2. Monometallic catalysts

The most studied catalysts for methanol decomposition are metallic: Cu, Ni, Pt and Pd [111–118]. In particular, Pt has been the subject of much scrutiny and controversy, namely due to the debate regarding the dissociation reaction pathway (figure 10). Using high-resolution electron loss spectroscopy and thermal desorption spectroscopy, the clean Pt(111) surface was reported to allow methanol decomposition into CO and H_2 at 140 K, while the same surface covered by oxygen instead forms water and methoxy (CH_3O), which then require a higher temperature to decompose into the final products (CO and H_2) [119]. This has been confirmed by several theoretical and experimental works [111–113, 120, 121]. Using different experimental techniques (secondary ion mass spectrometry and thermal programmed desorption), it has also been shown that methanol can decompose on Pt(111) by first breaking the C–O bond, forming a methyl group [122], a similar mechanism as the one reported at high temperatures on the (1 × 1)Pt(110) surface [123]. Regardless of the mechanism leading to the complete methanol decomposition, the greatest concern lies in the fact that

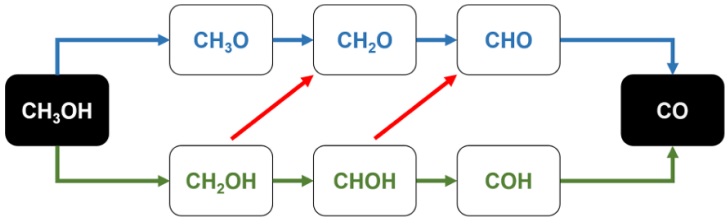

Figure 10. Representation of several reaction pathways for methanol decomposition. The two main pathways begin by breaking the O–H bond (blue) or the C–H bonds (green). Adapted from [131]. Copyright (2014), with permission from Elsevier.

CO adsorbs very strongly on the Pt surface, quickly reducing its catalytic capability [124–127]. This CO poisoning can be mitigated by mixing platinum with another metal, by surface coverage, alloying, doping, etc. The quest for a suitable combination served as motivation for most of the works on methanol decomposition on Pt, for at least the last decade [128–130].

2.3.3. Multimetallic catalysts

One of the most popular bimetallic catalysts for methanol decomposition is Au/Pt. One reason for this is that, on these bimetallic surfaces, the energy (and, consequently, the temperature) required for CO desorption reduces to less than a half of that on pure Pt. In fact, on Pt(111) and Pt(100), the CO desorption temperatures are 400 K and 525 K, corresponding to desorption energies of around 1.12 and 1.41 eV, respectively [132]. If, instead, one considers surfaces with the same Miller indexes, but with approximately one half of the surface Pt atoms substituted by Au atoms, the CO desorption temperatures are considerably lower (174 K and 237 K, respectively), and so are the desorption energies (0.46 and 0.62 eV, respectively) [133]. This result, predicted by DFT calculations and confirmed by TPD experiments, implies that Au/Pt bimetallic surfaces are not as easily poisoned by CO as pure Pt surfaces. The same study also showed that the Au/Pt surface is stable in the conditions required for CO desorption.

Yuan *et al* [117] employed DFT calculations to study methanol decomposition on the Au(111) surface, with some Au surface atoms replaced by Pt in an hexagonal fashion, and predict an alternative reaction mechanism, which ultimately may not lead to the production of CO. By comparing two general decomposition reaction paths—(a) breaking the O–H bond first vs (b) breaking it last—they found that the former contains one sizeable barrier to overcome, while the latter contains three (see figure 11 and table 2). In the same study, it was also shown that the two paths are very unlikely to cross each other in one of the intermediate reactions. The highest energy barrier for reaction path (a) is of 0.98 eV and corresponds to the O–H bond scission, while the ensuing C–H scissions require less energy. From the data in table 2, we can conclude that on PtAu(111), after CH_3OH becomes CH_3O, the latter should easily decompose to CH_2O, which is then harder to break. This contrasts with the clean Pt(111) surface where, after O–H scission, the decomposition reaction easily continues to form CO, due to the extremely lower energy barriers. The values in table 2 corresponding to methanol decomposition path (b) show that the alloying effect has quite a weak impact. Here it should be noted that the calculated adsorption energies of methanol on the Pt(111) and PtAu(111) surfaces are very low, 0.33 and 0.29 eV, respectively [112]. Both these values are lower than the energy barriers of the first reaction steps shown in table 2 and, therefore, methanol is more likely to desorb from the surface and lose its first H atom through some other mechanism, such as a collision, than when adsorbed. The reactions can then proceed on the catalytic surface because the absolute binding energies of both CH_3O and CH_2OH on either surface are all higher than 1.50 eV, favoring dehydrogenation rather than desorption, especially through path (a). One crucial difference between Pt(111) and PtAu(111) is the barrier for CH_2O dehydrogenation, which is much higher in the bimetallic surface. This difference, added to the moderate adsorption energy of CH_2O on PtAu(111) (0.54 eV), suggests that CH_2O could be directly oxidized by atmospheric oxygen into formic acid, instead of forming CO.

Pure Pt and Pt/Au clusters have also been theoretically studied in terms of methanol dehydrogenation and CO desorption [134]. Qualitatively, the results coincide with those of previous calculations and experiments [117, 129, 132]; it was found that, although on Pt/Au the energy of the dissociation rate-limiting step is harder to overcome, the final CO desorption is much easier on Pt/Au. On the Pt_3 cluster, the dissociation was predicted to begin with a C–H bond scission with an energy barrier of 0.56 eV, while on $PtAu_2$ the reaction begins by breaking the O–H bond, with an energetic cost of 0.93 eV. The latter is compensated by a CO desorption energy of 0.19 eV, much lower than the 1.31 eV calculated for Pt_3.

The alloying effect of Pt/Au on TiO_2 for methanol decomposition was finally studied in detail, both theoretically and experimentally, by Tenney *et al* [135]. There is indeed very strong synergy between all the

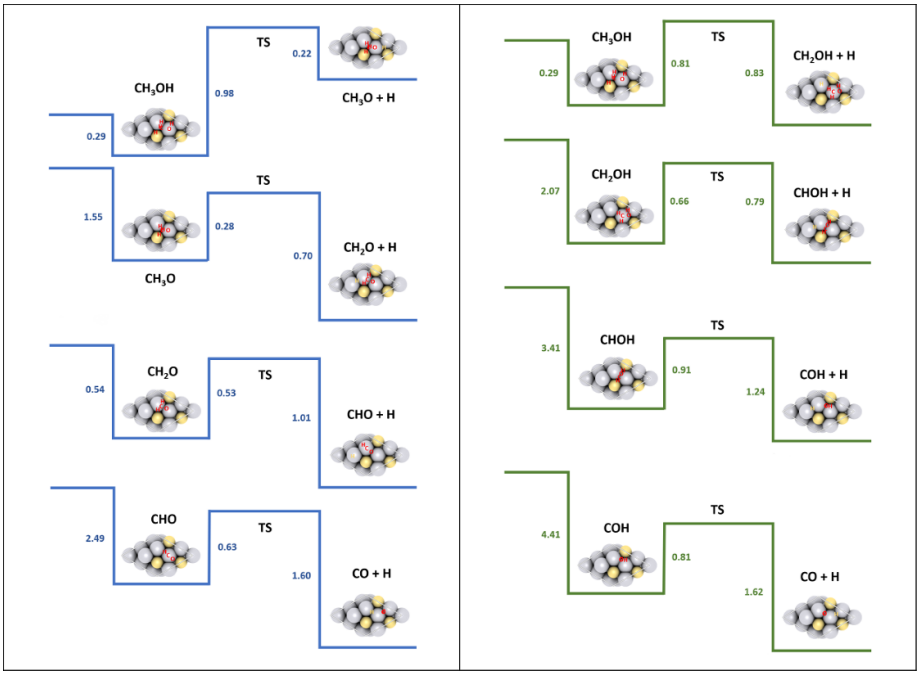

Figure 11. Visual representation of the methanol dehydrogenation process along two pathways, each beginning (left) or ending (right) with the O–H bond breaking. Color code for blue and green pathways as in figure 10. From top to bottom, hydrogen bonds in the adsorbed methanol molecule are sequentially broken until only CO is left. The numbers represent energies of adsorption, migration, or energy barriers. Gray and yellow spheres represent atoms of platinum or gold, respectively. Labels in red indicate the positions of the carbon, oxygen, or hydrogen atoms above the surface. Adapted from [117], with the permission of AIP Publishing.

Table 2. Energy barriers as calculated in [117], in eV, for methanol decomposition, following two paths: O–H bond breaking (a) as the first step vs (b) as the last step.

Reaction	Pt(111)	PtAu(111)
(a) Starting with O–H scission		
$CH_3OH \rightarrow CH_3O + H$	0.81	0.98
$CH_3O \rightarrow CH_2O + H$	0.25	0.28
$CH_2O \rightarrow CHO + H$	<0.10	0.53
$CHO \rightarrow CO + H$	0.23	0.63
(b) Ending with O–H scission		
$CH_3OH \rightarrow CH_2OH + H$	0.67	0.81
$CH_2OH \rightarrow CHOH + H$	0.63	0.66
$CHOH \rightarrow COH + H$	0.80	0.91
$COH \rightarrow CO + H$	0.97	0.81

materials involved. It was shown that Pt/Au clusters with more than 50% Au contain only Au atoms on the surface. As previous studies had found, the first bond to be broken in the process is O–H, a scission facilitated by the presence of TiO_2. However, if only TiO_2 was present, the resulting methoxy (CH_3O) would likely recombine with the hydrogen and desorb without reaction. The role of Au is to promote H_2 desorption at low temperature (<300 K) to prevent the reaction from stopping at this stage. The reaction on pure Au clusters yields CH_2O rather than CO as its main product. Nevertheless, on Pt/Au, CH_3O connects to the surface via its O atom, which induces the migration of Pt from under Au to the surface and allows the dehydrogenation to complete. The dehydrogenation activity of this cluster is very similar to that of pure Pt clusters. The advantage of the alloy is that the CO desorption temperature decreases with increasing Au fraction (in particular, it decreases by about 25 K at an Au fraction of 25%) [136]. Therefore, a delicate balance between the amount of Pt and Au needs to be found: if there is too much Au, the dehydrogenation will not be completed, but too much Pt yields too strong a binding energy for CO, poisoning the catalyst.

Let us now turn our attention to bimetallic catalysts with Pt and metals other than Au. Guo *et al* studied the substitutional doping of Ni on Pt [131]. This doping was found to shift the dehydrogenation path from first breaking one C–H bond to begin with an O–H bond scission. Charge transfer from Ni to Pt was found to weaken the CO poisoning. Removing CO from the PtNi cluster was predicted to require 0.85 eV, while the same operation on Pt was calculated at between 0.89 and 1.51 eV. More recently, a theoretical study on the

PtRu(111) surface over boron-doped graphene found that adding Ru to Pt weakens the CO adsorption, and that the graphene sheet improves the catalytic activity by lowering the methanol dehydrogenation energy barriers [137, 138]. The CO adsorption energy on PtRu(111) on boron-graphene was calculated at −1.81 eV, which is considerably lower than on Ru(0001) (−2.30 eV [139]) or PtRu(111) (−2.10 eV [140]). Also, recently, Pt/Ir was demonstrated as an alternative catalyst for methanol decomposition with reduced CO poisoning with respect to pure Pt, with two advantages: weaker CO binding energy (by 0.26 eV) and more favorable CO oxidation by OH^-.

It should be noted that catalysts involving noble metals, such as Ru, Ir, Pt, or Au, may not realistically be employed at a significant scale. However, they can be regarded as benchmarks, whose performance as catalysts may be achieved or surpassed by research on mono or multimetallic catalysts. Therefore, it is not surprising to see that other researchers devoted their attention to alloying of noble metals with abundant ones as Cu, Ni or Co. Upon a combination of DFT calculations and thermochemical scaling relationships, Mehmood *et al* [141] estimated the thermochemistry and kinetics of the methanol decomposition on pure metallic or bimetallic clusters with four *M* atoms (*M* = Ag, Au, Co, Cu, Rh, Pd and Pt). From a volcano plot of the methanol decomposition using the adsorption energies of O and C as descriptors, they found that the Pd_1Cu_3 and Pd_2Co_2 subnanometer metal clusters were close to the predicted maximum of the volcano, with predicted rates higher than those predicted for Rh_4, Pd_4 or Pt_4 clusters. Further research is certainly needed to analyze whether it is possible to develop improved catalysts based on abundant metals for the methanol decomposition reaction.

2.4. Ammonia decomposition

2.4.1. Introduction

Around 150 million tons of ammonia (NH_3) are produced every year around the world [11]. This compound has long been known as an excellent choice for hydrogen production, storage and transport. Indeed, liquid ammonia contains 17.8 wt% hydrogen, amounting to 50% more hydrogen per volume than liquid hydrogen itself [142]. The fact that a pressure of around 10 atm is enough to liquefy ammonia at 298 K makes its liquid-phase storage relatively cheap, decreases the size and weight of containers, and allows for a simple way to store hydrogen at a higher volumetric density than liquid H_2.

The global reaction of ammonia (NH_3) decomposition to form hydrogen (H_2),

$$2NH_3 \rightarrow N_2 + 3H_2 \tag{9}$$

is endothermic, and the corresponding enthalpy of reaction at 298 K is 91.86 kJ mol^{-1}, or nearly 1 eV. High temperatures and low pressures facilitate this process, and in practice this reaction is normally performed at around 850 °C [12]. Alternatives include burning a fraction of the resulting hydrogen in order to help maintain the high temperature. The trade-off is the reduction of the reaction yield, as some of the hydrogen is replaced by the product(s) of combustion and water vapor, even if the combustion is done in a carbon-free atmosphere to prevent the formation of side products such as carbon monoxide or dioxide [12].

2.4.2. Monometallic catalysts

In reality, ammonia decomposition reaction occurs in steps, where NH_3 is successively dehydrogenated, forming N and H, which recombine as N_2 and H_2, respectively [143],

$$NH_3 + * \rightarrow NH_3^* \tag{10}$$

$$NH_3^* + * \rightarrow NH_2^* + H^* \tag{11}$$

$$NH_2^* + * \rightarrow NH^* + H^* \tag{12}$$

$$NH^* + * \rightarrow N^* + H^* \tag{13}$$

$$N^* + N^* \rightarrow N_2 + 2* \tag{14}$$

$$H^* + H^* \rightarrow H_2 + 2*. \tag{15}$$

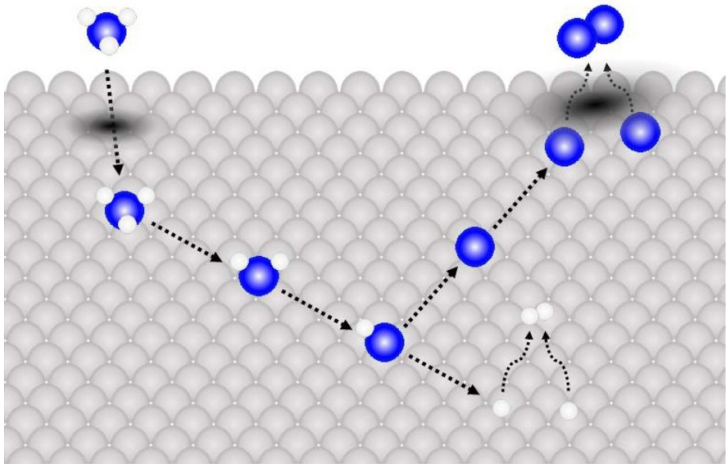

Figure 12. Representation of the general mechanism of ammonia adsorption, decomposition, and product desorption on a catalyst surface. The blue and white spheres represent nitrogen and hydrogen atoms, respectively, while the remaining spheres are surface atoms. Adapted with permission from [144]. Copyright (2019) American Chemical Society.

These reactions represent, respectively, the adsorption of ammonia, the first, second and third dehydrogenations of adsorbed ammonia, and the recombination and desorption of two nitrogen or hydrogen adatoms (as shown in figure 12). A suitable catalyst must therefore be such that the binding of the nitrogen atom of NH_x is strong enough for the dehydrogenation to occur, but weak enough to allow the resulting nitrogen adatoms to recombine as N_2 and desorb from the surface. This trade-off is crucial in finding the ideal catalyst for ammonia decomposition.

In this review, we focus on metallic catalysts (which, in fact, are currently the default choice) but, in the case of ammonia decomposition for hydrogen production, other choices, such as nitrides and carbides of Co, Cr, Fe, Mn, Ni, Ti and V, or alkali metal amides are available. The former have been found to show catalytic activity similar to that of metals [145, 146], while the latter seem promising to promote ammonia decomposition at temperatures lower than 450 °C, contrasting with the temperatures above 600 °C required to achieve 100% conversion efficiency on metal catalysts. For further details on ammonia decomposition on non-metallic catalysts, please refer to the very recent reviews of Lamb *et al* [11] and Mukherjee *et al* [147].

Ammonia decomposition using metallic catalysts has been investigated for so long that the activity trend for different metals has been known since 1823, before the word 'catalysis' was applied to these processes [148, 149]. Metallic catalysts for ammonia decomposition are so well established that some works do not even mention other types of catalysts. According to Häussinger *et al* [12], the typical catalysts are nickel- or iron-based. However, other metals present higher catalytic activity. The list of studied monometallic catalysts increased over time and, in 2004, Ganley *et al* experimentally probed the activity of 13 metals supported over alumina (Al_2O_3) at $T = 580$ °C [150], measured as TOFs, and with results summarized in table 3. In all theoretical and experimental works, the consensus is that ruthenium yields the highest catalytic activity among all monometallic catalysts, as shown in figure 13. Other studies give slightly different orders, depending on the support, but Ru retains its merit [151, 152]. Nevertheless, research did not end here, as it was found that the activity of Ru at lower temperatures decreases considerably. For instance, at 450 °C, the TOF of Ru supported on carbon nanotubes becomes less than 50% [153].

While in ammonia synthesis via the Haber–Bosch process, the rds is known to be the dissociation of the N_2 triple bond, the limiting step in ammonia decomposition depends on the metallic catalyst. On precious metals, such as Ru, Rh, Ir or Pd, the rds is the breaking of N–H bonds, while for nonprecious metals, like Ni, Co or Fe, the limiting step is N_2 desorption, one of the last steps of the process [155]. This is the reason behind the famous 'volcano plot' obtained in [154], which correlates the catalytic activity of several metals with the energy barrier for N–H bond scission. This plot shows that such a correlation exists separately for precious and nonprecious metals: the TOF increases with the N–H bond scission activation energy on the latter and decreases on the former [147, 151, 154]. The adsorption energy of nitrogen on each metal correlates as a volcano with both the TOF for ammonia synthesis and ammonia decomposition (with shifted maxima), and shows that Ru is the best catalyst for both processes among pure metals [151]. The volcano shape implies that there is an ideal value for nitrogen binding energy which leads to the highest ammonia synthesis activity. With this in mind, in 2005, Boisen *et al* [152] predicted that a combination of two metals

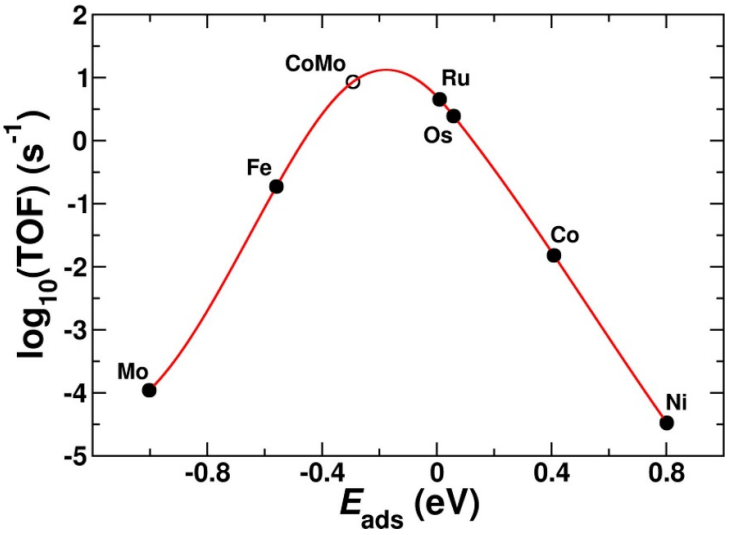

Figure 13. Calculated TOF for ammonia synthesis as a function of the nitrogen adsorption energy, catalyzed by monometallic or bimetallic CoMo surfaces. Adapted with permission from [154]. Copyright (2001) American Chemical Society.

Table 3. Measured ammonia decomposition TOF over several metal catalysts [150]. Reprinted with permission from Springer Nature Customer Service Centre GmbH: Springer Nature, Catalysis Letters [150] © 2004.

Catalyst	TOF (s^{-1})
Ru	6.85
Ni	4.21
Rh	2.26
Co	1.33
Ir	0.786
Fe	0.327
Pt	0.0226
Cr	0.0220
Pd	0.0194
Cu	0.0130
Te	<0.0056
Se	<0.0044
Pb	<0.0024

(one where the N adsorption energy is too high and another where it is too low), such as CoMo, should display an activity close to the optimal one (see figure 13). Their experiments confirmed that, at low NH_3 concentrations, CoMo displays a better catalytic activity for ammonia synthesis than Co or Mo individually, and better than Ru. This bimetallic mixture, supported on MCM-41 (Mobil composition of matter No. 41 type silica), was later also used for ammonia decomposition and, in this case, an ideal Co/Mo ratio of 7/3 was found [156]. This process of combining two elements hoping to obtain properties intermediate between the original ones was called 'periodic table interpolation' and suggested to be a general phenomenon in the field of catalysis, in reactions where the catalytic activity does not change monotonically with the interaction energy, such as the case of volcano-like relationships. In addition, the interpolation will only produce the desired effect if the resulting surface contains both chemical elements. If, as usually happens, one of the elements becomes too dominant on the surface, either due to the intrinsic properties of the mixture or due to interacting too strongly with the adsorbate, the interpolated properties might not be observed [157]. This ground-breaking work motivated the prediction of the ammonia decomposition activity of bimetallic catalysts, based on periodic table interpolation.

2.4.3. Multimetallic catalysts

Encouraged by the success of Boisen *et al* in producing a bimetallic catalyst for ammonia decomposition with better activity than Ru via periodic table interpolation of the volcano plot, scientists began studying other combinations of metals using both computational and experimental techniques.

In 2010, Hansgen *et al* studied theoretically and experimentally several configurations of Ti, V, Cr, Mn, Fe, Co, and Ni [143]. The catalytic activity for ammonia decomposition was compared on surfaces containing

Table 4. Calculated nitrogen binding energies of some TMs on platinum [143, 158]. The second and third columns show the values for a single layer of the metal (*M*) on the subsurface and on the surface of platinum (Pt), respectively, in kcal/mol. The last column shows values for monometallic systems.

Metal	Pt–*M*–Pt	*M*–Pt–Pt	*M*
Pt	—	—	102.1
Ti	70.7	176.1	—
V	81.0	188.1	—
Cr	76.3	188.3	—
Mn	77.6	207.2	—
Fe	78.4	134.1	155.3
Co	83.4	126.5	119.3
Ni	87.5	130.7	113.8
Cu	93.1	86.6	74.5

only these metals, or made up of one layer of one of the metals over Pt, both on the surface (denoted *M*–Pt–Pt, where *M* denotes a TM) and on the subsurface, under a single layer of Pt (denoted Pt–*M*–Pt). Several crucial conclusions were taken after this study. Interpolation of the points of the volcano plot indicates that its peak (where the maximum TOF is achieved) is located at an N adsorption energy of around 134 kcal mol^{-1}; this is slightly lower than the 141.6 kcal mol^{-1} attributed to Ru. The bimetallic surfaces were found to fit well into the volcano relationship; therefore, the study proceeds to finding a TM which, when over Pt, displays an N binding energy close to 134 kcal mol^{-1}. The results are summarized in table 4.

On the one hand, all of the subsurface configurations showed nitrogen binding energies below 90 kcal mol^{-1}, so they were discarded as catalysts for ammonia decomposition. On the other hand, a single layer of some of the metals over Pt showed very promising results. While one layer of Ti, V, Cr or Mn on Pt gives too high a binding energy (above 175 kcal mol^{-1}), the surfaces of Ni–Pt–Pt, Co–Pt–Pt and Fe–Pt–Pt have binding energies remarkably close to the ideal value of 134 kcal mol^{-1}. These authors synthesized the Ni/Pt bimetallic system by depositing Ni at room temperature or at 600 K, which led to the Ni–Pt–Pt or to the Pt–Ni–Pt configurations, respectively. These systems were then studied using TPD and high-resolution electron energy loss spectroscopy. The Ni–Pt–Pt surface was shown computationally (and later experimentally) to be more stable than the subsurface one (e.g. Pt–Ni–Pt). Furthermore, upon exposure to oxygen, the subsurface configuration rearranged itself into the surface one, both at low pressures (around 10^{-10} bar) and at atmospheric pressure [159–161]. The experiments also confirmed other theoretical predictions: the Ni–Pt–Pt surface was found to be very active for ammonia decomposition, as both its nitrogen desorption temperature and ammonia dehydrogenation barrier (the two rate-determining steps in ammonia decomposition) are lower than those of Ru. This surface was predicted to display activity for steady-state decomposition below 600 K.

Similarly to Ni–Pt–Pt, the N binding energies on Co–Pt–Pt and Fe–Pt–Pt surfaces are very close to the desired value of 134 kcal mol^{-1}. In table 4, Cu/Pt is the only bimetallic combination for which both Pt–*M*–Pt and *M*–Pt–Pt configurations represent an improvement towards reaching the desired N adsorption value of 134 kcal mol^{-1}, when compared to the corresponding monometallic catalyst. In contrast, for Fe, Co and Ni, only the *M*–Pt–Pt configuration shows an advance towards 134 kcal mol^{-1}, while the Pt–*M*–Pt configuration displays a value farther from 134 kcal mol^{-1} than the monometallic catalyst. For this reason, Co–Pt–Pt, Fe–Pt–Pt, and both Cu multimetallic surfaces were analyzed by the same group in another work [158]. In that study, it was confirmed that the N binding energy correlates well with the catalytic activity of bimetallic systems, and it was found that Cu bimetallic surfaces are inadequate for ammonia decomposition. In contrast, the Co/Pt and Fe/Pt were predicted to be more active catalysts for ammonia decomposition than the corresponding monometallic materials. Unlike the case of Ni–Pt–Pt, the surface configurations of Cu/Pt, Co/Pt and Fe/Pt are not always the most stable ones when compared to the subsurface structures. In fact, the Pt–Cu–Pt stacking is the most stable one regardless of the surface nitrogen coverage, while, according to the calculations, the Co–Pt–Pt and Fe–Pt–Pt configurations are only the ground state for nitrogen coverages of over 0.35 ML. Since the subsurface configurations are ineffective at decomposing ammonia, the reaction needs to occur at nitrogen coverages above this value in order to stabilize the *M*–Pt–Pt configuration. As stated by the authors, the experiments were carried out under ultrahigh vacuum, where the nitrogen coverage saturation is around 0.3 ML, hampering the stabilization of the desired surface configuration. There is, however, hope in the form of material edges and defects, which were not taken into account in the calculations, as these likely affect the thermodynamic and kinetic relative stability of the surface and subsurface configurations [162, 163].

Table 5. Energy barriers, in kcal/mol, for the scission of NH_x–H bonds, when adsorbed on different surfaces.

Surface	$NH_3^* \rightarrow NH_2^* + H^*$	$NH_2^* \rightarrow NH^* + H^*$	$NH^* \rightarrow N^* + H^*$
Pt	21.6	19.9	5.7
Fe	12.2	17.2	2.7
Co	18.9	19.1	4.6
Cu	34.2	21.0	7.8
Pt–Fe–Pt	32.2	20.9	7.5
Fe–Pt–Pt	16.2	18.3	3.8
Pt–Co–Pt	29.6	20.7	7.1
Co–Pt–Pt	17.6	18.7	4.2
Pt–Cu–Pt	24.5	20.3	6.3
Cu–Pt–Pt	27.9	20.6	6.8

The energy barriers for N–H bond scissions, despite not being the rate-determining step for ammonia decomposition on nonprecious metals, also play a relevant role in the process and as a matter of fact correlate approximately linearly with the corresponding TOF. The dehydrogenation energy barriers on selected surfaces [159], calculated using the method described in [164], are shown in table 5. These barriers are significantly lower than, for instance, the ones calculated for Pd–Cu, or for Pd-doped Cu(100) [165, 166], but similar to the calculations of Novell-Leruth *et al* for Pt, Pd and Rh [167]. If one excludes the monometallic Cu surface, all linear correlation coefficients between the values in tables 4 and 5 are above 0.95 implying that, on surfaces with higher N adsorption energies, the NH_3 dehydrogenation energy barriers are lower. This also hints that, like the N binding energies, these barriers can be used to predict the TOF of ammonia decomposition on bimetallic surfaces.

All kinds of combinations of metals under different conditions are still being tested, as ammonia decomposition on multimetallic catalysts is an extremely hot topic. In the following paragraphs, we examine some works that were published very recently.

Huang *et al* compared the performance of Ni, Co and Ni/Co metallic catalysts supported on $Ce_{0.6}Zr_{0.3}Y_{0.1}O_2$ (CZY) [168]. It was found that the TOF is maximized at a Ni/Co mass ratio of 1/9. The resulting TOF of around 0.67 s^{-1} is higher than the ones measured for Ni or Co on CZY (0.52 and 0.54 s^{-1}, respectively), but still much lower than the TOF on some monometallic catalysts (see table 3). This higher catalytic activity was attributed to an increase in surface area.

An experimental comparison between the catalytic activity of Ni, Ru and Ni/Ru supported on Al_2O_3 and CeO_2 showed that the initial activity of Ru/CeO_2 is the highest among all the analyzed combinations but, as happens with all studied Ru-containing catalysts, it deactivates too early due to metal sintering in the case of Ru/Al_2O_3 or Ru volatilization on Ru/CeO_2 [169]. Additionally, CeO_2 was demonstrated to be a better support for ammonia decomposition catalysts than Al_2O_3. The Ni/CeO2 catalyst (with a TOF of 0.03 s^{-1} at 400 °C, lower than the 0.4 s^{-1} measured on Ni/SiO_2 at the same temperature [170]) ended up being the recommended one, due to its higher activity and catalytic stability, along with its lower cost, and because the bimetallic $Ni/Ru/CeO_2$ showed no improvement over Ru/CeO_2. Around the same time, Vacharapong *et al* tried a similar approach: a Ni catalyst over an Al_2O_3 support doped with Ce, including magnetic inducement (to aid in controlling the composition and uniformity of Ce) [171]. Both the doping and the magnetic field were found to increase the ammonia conversion percentage and TOF. When both changes are taken into account, the ammonia conversion percentages measured on magnetically induced Ni on Ce-doped Al_2O_3 were almost twice as high as on Ni/Al_2O_3, with the largest effect coming from the doping rather than from the magnetic inducement.

The plasma-assisted ammonia decomposition catalytic activities of monometallic Fe, Co, Ni and Mo catalysts were compared with those of some of their bimetallic combinations (Fe–Co, Mo–Co, Fe–Ni and Mo–Ni), deposited on SiO_2 [172]. In terms of ammonia conversion percentage, Co proved to be the best among the monometallic catalysts, and Fe–Ni the best among the bimetallic ones, with NH_3 conversions of 48% and 60%, respectively, at 460 °C. Curiously, Fe–Ni was the only bimetallic surface which displayed a higher conversion percentage than the parent metals, at any temperature between 330 °C and 460 °C. Given its promising capabilities, Fe–Ni was then tested with different molar ratios, and the activity was found to peak at 61% on 6Fe–4Ni, showing excellent durability over a 200 h long period of continuous operation. The 6Fe–4Ni catalyst also exhibited the highest synergy with plasma: at 500 °C, over 99.9% of ammonia was decomposed, at a TOF of around 3.46 s^{-1}. Optical emission spectra characterization showed that plasma pre-activates NH_3 into NH_2 and NH and accelerates both the initial ammonia adsorption on metals and the final recombinative desorption of N adatoms. Consequently, the combination of plasma technology with a relatively cheap metal catalyst proved promising in the quest for better catalysts for ammonia decomposition.

One of the most recent studies involves quinary nanoparticles made up of Co, Mo, Fe, Ni and Cu [173]. Tests at 500 °C revealed that the ammonia conversion percentage and the TOF critically depend on the Co/Mo ratio, with a volcano-type relationship with the N adsorption energy. While for ratios $\leqslant 1$ the TOF was found lower than on Ru/TiO_2 (3.08 s^{-1}), including more Co than Mo resulted in TOFs of 5.45 and 7.00 s^{-1} for ratios of 9/5 and 11/3, achieving conversions of 64.5% and 100%, respectively. The Co/Mo ratio in these quinary nanoparticles can therefore be adjusted to optimize their catalytic activity under different experimental conditions.

3. Final remarks and future directions

The review of the literature concerning the utilization of multimetallic catalysts in some important reactions for H_2 production shows that the added metals have different roles in the catalytic processes. The metal alloying alters the band structure, which necessarily changes the reactivity of the material, leading to different catalysis-relevant changes, such as adsorption mechanisms and strength, as well as alternative surface reaction paths. The supports have been found to also have important roles in the reactions: by competing with the metallic particles for adsorption of some intermediate species, the poisoning of active metal sites can be avoided; in other cases, the support induces changes in the catalytic properties of the metal particles which are beneficial.

In the case of the WGSR, an important synergic effect was found when alloying copper and nickel. While the shift activity of nickel is greater than that of copper, nickel is found to be less selective and some formation of methane occurs. The alloying of the two metals leads to high reaction rates while retaining methane formation, i.e. copper is essential to control the high activity of nickel towards the cleavage of the C–O bond of carbon monoxide, thus suppressing undesirable side effects. Results of computational studies suggest that the incorporation of very small amounts of other abundant metals, e.g. Zn or Al, may dramatically improve the activity of copper towards the WGSR. The addition of Zn shifts to lower values the reduction temperature of CuO to Cu while the main role of Al is to increase the catalyst stability. In the case of the supported catalysts, catalysts using reducible oxide supports are much more active than those employing non-reducible oxides.

The steam reforming of hydrocarbons relies essentially on nickel-based catalysts. However, these catalysts are prone to coke formation. This problem can be somewhat prevented upon the utilization of high H_2O/CH_4 ratios but, unfortunately, this generates increased costs in post-reaction separations. Therefore, it is of utmost importance to find catalysts that can oxidize adsorbed carbon into CO. Multimetallic catalysts alloying nickel with not only noble metals, such as gold, platinum, or silver, but Earth-abundant metals such as copper and cobalt have also been suggested in the literature to inhibit coke formation while retaining or increasing activity. Apparently, the metal element added to the nickel catalyst prefers to interact with very low-coordinated Ni atoms, which are highly reactive sites that promote formation of carbon deposits. Therefore, in this specific catalytic process, the added metals do not lead to an increase of the intrinsic activity of nickel towards the steam reforming but have an important role of avoiding coke formation, improving the stability and resistance of the catalyst.

Traditionally, Pt is the most studied and promising catalyst for methanol decomposition into hydrogen and carbon monoxide. One major problem of using pure Pt is the quick CO poisoning of its surface, caused by strong CO adsorption. This motivated the still ongoing research of multimetallic alternatives, which attempt to keep the catalytic potential of monometallic surfaces for dehydrogenating methanol, while mitigating the CO saturation. Among these, Pt/Au is quite popular for its success in greatly reducing CO poisoning and in some cases providing reaction paths which avoid the production of CO.

Studies of bimetallic materials as catalysts for ammonia decomposition show that they have the potential to be more active than Ru-based materials. New combinations of metals and technologies are still being discovered, with the material design being further complicated by the unpredictability of some properties. While some of the studies reviewed here used the simple periodic table interpolation to form bimetallic compounds, this approach sometimes yields results worse than those of the parent metals. Employing first-principles calculations to predict and tune nitrogen binding energies has been shown to often lead in the desired direction, due to the established volcano-like relationship between this quantity and the TOF of catalysts. However, this area is still relatively new and further tests are still needed to confirm the reproducibility and stability of the results available so far.

Regrettably, the unifying feature of some of these reactions is the reliance on precious metals, given their resistance against oxidation and selectivity. Naturally, since these metals are rare by definition, more sustainable alternatives are required. This motivates the use of first-row TMs, such as Cu- and Ni-based bimetallic materials. Encouragingly, these non-precious TMs are also catalytically active, in special when alloyed with other Earth-abundant metals which can lead to further improvements if when wisely combined.

Despite the significant knowledge gathered from the experimental and computational studies reported in the literature, additional work is needed. Experimentally, studies are needed to fully understand the compositions of the catalysts under *operando* conditions, either the support termination, its interface with the metal particles and the amount of segregation at the surface of the metal particles. This information is crucial for developing structural models that can be used in parallel computational studies. In our view, the synergic combination of experimental and computational works is important to advance from trial and error synthesis to *de facto* tailored design of catalysts.

Data availability statement

No new data were created or analyzed in this study.

Acknowledgments

This work was developed within the scope of the project CICECO-Aveiro Institute of Materials, Refs. UIDB/50011/2020 and UIDP/50011/2020, financed by national funds through the Fundação para a Ciência e a Tecnologia (FCT/MCTES) and co-financed by FEDER (European Regional Development Fund) under the PT2020 Partnership Agreement. DG is thankful to project SILVIA with reference CENTRO-01-0145-FEDER-31002. This publication is based upon work from COST Action 18234, supported by COST (European Cooperation in Science and Technology).

ORCID iDs

Rui V Afonso https://orcid.org/0000-0001-9131-3237
José D Gouveia https://orcid.org/0000-0002-5099-7772
José R B Gomes https://orcid.org/0000-0001-5993-1385

References

[1] The North American Council for Freight Efficiency 2020 Hydrogen color spectrum *NACFE December 2020 Newsletter*
[2] Tao L, Choksi T S, Liu W and Pérez-Ramírez J 2020 Synthesizing high-volume chemicals from C_2 without direct H_2 input *ChemSusChem* **13** 6066–89
[3] The Royal Society 2017 The potential and limitations of using carbon dioxide (available at: https://royalsociety.org/-/media/policy/projects/carbon-dioxide/policy-briefing-potential-and-limitations-of-using-carbon-dioxide.pdf) (Accessed 25 March 2021)
[4] Rao P C and Yoon M 2020 Potential liquid-organic hydrogen carrier (LOHC) systems: a review on recent progress *Energies* **13** 6040
[5] Chen L, Qi Z, Zhang S, Su J and Somorjai G A 2020 Catalytic hydrogen production from methane: a review on recent progress and prospect *Catalysts* **10** 858
[6] The Royal Society 2020 Ammonia: zero-carbon fertiliser, fuel and energy store (available at: https://royalsociety.org/topics-policy/projects/low-carbon-energy-programme/green-ammonia/) (Accessed 25 March 2021)
[7] Zhao X, Joseph B, Kuhn J and Ozcan S 2020 Biogas reforming to syngas: a review *iScience* **23** 101082
[8] Chen W H and Chen C Y 2020 Water gas shift reaction for hydrogen production and carbon dioxide capture: a review *Appl. Energy* **258** 114078
[9] Araiza D G, Gómez-Cortés A and Díaz G 2020 Methanol decomposition over bimetallic Cu-M catalysts supported on nanoceria: effect of the second metal on the catalytic properties *Catal. Today* **356** 440–55
[10] Garcia G, Arriola E, Chen W H and de Luna M D 2021 A comprehensive review of hydrogen production from methanol thermochemical conversion for sustainability *Energy* **217** 119384
[11] Lamb K E, Dolan M D and Kennedy D F 2019 Ammonia for hydrogen storage; A review of catalytic ammonia decomposition and hydrogen separation and purification *Int. J. Hydrogen Energy* **44** 3580–93
[12] Häussinger P, Lohmüller R and Watson A M 2012 Hydrogen, 2. Production *Ullmann's Encyclopedia of Industrial Chemistry* (Weinheim, Germany: Wiley-VCH Verlag GmbH & Co. KGaA) pp 249–307
[13] Santhanam K S V, Press R J, Miri M J, Bailey A V and Takacs G A 2018 *Introduction to Hydrogen Technology* (Hoboken, NJ: John Wiley & Sons Inc)
[14] Speight J G 2011 Production of hydrocarbons from natural gas *Handbook of Industrial Hydrocarbon Processes* ed J G Speight (Oxford: Elsevier) pp 127–62
[15] Fierro J L G, Peña M A and Alvarez-Galvan M C 2011 Supported metals in the production of hydrogen *Catalytic Science Series | Supported Metals in Catalysis* vol 11, ed J A Anderson and M Fernández-García (London: Imperial College Press) pp 301–405
[16] Gao J, Hou Z, Lou H and Zheng X 2011 Dry (CO_2) reforming *Fuel Cells: Technologies for Fuel Processing* ed D Shekhawat, J J Spivey and D A Berry (Oxford: Elsevier) pp 191–221
[17] de Vasconcelos S M, de Souza A E Á M, Araújo M S, Silva M A M, Araújo F A D, de Lima Filho N M and Abreu C A M 2019 Effect of the light alkane content of natural gas on the production of hydrogen and coke during the dry reform *J. Adv. Chem. Eng.* **9** 191
[18] Wu H, La Parola V, Pantaleo G, Puleo F, Venezia A and Liotta L 2013 Ni-based catalysts for low temperature methane steam reforming: recent results on Ni-Au and comparison with other Bi-metallic systems *Catalysts* **3** 563–83
[19] Mortensen P M and Dybkjær I 2015 Industrial scale experience on steam reforming of CO_2-rich gas *Appl. Catal.* A **495** 141–51

[20] Aramouni N A K, Touma J G, Tarboush B A, Zeaiter J and Ahmad M N 2018 Catalyst design for dry reforming of methane: analysis review *Renew. Sustain. Energy Rev.* **82** 2570–85

[21] García-Diéguez M, Herrera C, Larrubia M Á and Alemany L J 2012 CO_2-reforming of natural gas components over a highly stable and selective NiMg/Al_2O_3 nanocatalyst *Catal. Today* **197** 50–7

[22] Liu Y, Wu Y, Akhtamberdinova Z, Chen X, Jiang G and Liu D 2018 Dry reforming of shale gas and carbon dioxide with Ni-Ce-Al_2O_3 catalyst: syngas production enhanced over Ni-CeO_x formation *ChemCatChem* **10** 4689–98

[23] Li X, Yan B, Yao S, Kattel S, Chen J G and Wang T 2018 Oxidative dehydrogenation and dry reforming of *n*-butane with CO_2 over NiFe bimetallic catalysts *Appl. Catal.* B **231** 213–23

[24] Arcotumapathy V, Vo D V N, Chesterfield D, Tin C T, Siahvashi A, Lucien F P and Adesina A A 2014 Catalyst design for methane steam reforming *Appl. Catal.* A **479** 87–102

[25] Hassan-Legault K, Mohan O and Mushrif S H 2019 Molecular insights into the activity and stability of popular methane reforming catalysts using quantum mechanical tools *Curr. Opin. Chem. Eng.* **26** 38–45

[26] Jones G *et al* 2008 First principles calculations and experimental insight into methane steam reforming over transition metal catalysts *J. Catal.* **259** 147–60

[27] Luna E C, Becerra A M and Dimitrijewits M I 1999 Methane steam reforming over rhodium promoted Ni/Al_2O_3 catalysts *React. Kinet. Catal. Lett.* **67** 247–52

[28] Guo X, Liu H, Wang B, Wang Q and Zhang R 2015 Insight into C + O(OH) reaction for carbon elimination on different types of CoNi(111) surfaces: a DFT study *RSC Adv.* **5** 19970–82

[29] Arevalo R L, Aspera S M, Escaño M C S, Nakanishi H and Kasai H 2017 Tuning methane decomposition on stepped Ni surface: the role of subsurface atoms in catalyst design *Sci. Rep.* **7** 13963

[30] Roy S, Hariharan S and Tiwari A K 2018 Pt–Ni subsurface alloy catalysts: an improved performance toward CH_4 dissociation *J. Phys. Chem.* C **122** 10857–70

[31] Ibrahim A A 2018 Hydrogen production from light hydrocarbons *Advances in Hydrogen Generation Technologies* ed M Eyvaz (London: InTech) pp 39–62

[32] Angeli S D, Monteleone G, Giaconia A and Lemonidou A A 2014 State-of-the-art catalysts for CH_4 steam reforming at low temperature *Int. J. Hydrog. Energy* **39** 1979–97

[33] Pleth Nielsen L, Besenbacher F, Stensgaard I, Laegsgaard E, Engdahl C, Stoltze P, Jacobsen K W and Nørskov J K 1993 Initial growth of Au on Ni(110): surface alloying of immiscible metals *Phys. Rev. Lett.* **71** 754–7

[34] Holmblad P M 1996 Modification of Ni(111) reactivity toward CH_4, CO, and D_2 by two-dimensional alloying *J. Chem. Phys.* **104** 7289–95

[35] Kratzer P, Hammer B and Nørskov J K 1996 A theoretical study of CH_4 dissociation on pure and gold-alloyed Ni(111) surfaces *J. Chem. Phys.* **105** 5595–604

[36] Holmblad P M, Hvolbæk Larsen J, Chorkendorff I, Pleth Nielsen L, Besenbacher F, Stensgaard I, Lægsgaard E, Kratzer P, Hammer B and Nørskov J K 1996 Designing surface alloys with specific active sites *Catal. Lett.* **40** 131–5

[37] Besenbacher F, Chorkendorff I, Clausen B S, Hammer B, Molenbroek A M, Nørskov J K and Stensgaard I 1998 Design of a surface alloy catalyst for steam reforming *Science* **279** 1913–5

[38] Hyldtoft J, Norskov J and Clausen B S 1998 Process for steam reforming of hydrocarbons (U.S. Patent #5,997,835)

[39] Molenbroek A M, Nørskov J K and Clausen B S 2001 Structure and reactivity of Ni-Au nanoparticle catalysts *J. Phys. Chem.* B **105** 5450–8

[40] Bengaard H S, Nørskov J K, Sehested J, Clausen B S, Nielsen L P, Molenbroek A M and Rostrup-Nielsen J R 2002 Steam reforming and graphite formation on Ni catalysts *J. Catal.* **209** 365–84

[41] Rostrup-Nielsen J R 1984 Sulfur-passivated nickel catalysts for carbon-free steam reforming of methane *J. Catal.* **85** 31–43

[42] Andersen N T, Topsøe F, Alstrup I and Rostrup-Nielsen J R 1987 Statistical models for ensemble control by alloying and poisoning of catalysts. I. Mathematical assumptions and derivations *J. Catal.* **104** 454–65

[43] Abild-Pedersen F, Lytken O, Engbæk J, Nielsen G, Chorkendorff I and Nørskov J K 2005 Methane activation on Ni(111): effects of poisons and step defects *Surf. Sci.* **590** 127–37

[44] Chin Y H (Cathy), King D L, Roh H S, Wang Y and Heald S M 2006 Structure and reactivity investigations on supported bimetallic Au–Ni catalysts used for hydrocarbon steam reforming *J. Catal.* **244** 153–62

[45] Triantafyllopoulos N C and Neophytides S G 2006 Dissociative adsorption of CH_4 on NiAu/YSZ: the nature of adsorbed carbonaceous species and the inhibition of graphitic C. formation *J. Catal.* **239** 187–99

[46] Keane M A, Gómez-Quero S, Cárdenas-Lizana F and Shen W 2009 Alumina-supported Ni–Au: surface synergistic effects in catalytic hydrodechlorination *ChemCatChem* **1** 270–8

[47] Niakolas D K, Ouweltjes J P, Rietveld G, Dracopoulos V and Neophytides S G 2010 Au-doped Ni/GDC as a new anode for SOFCs operating under rich CH_4 internal steam reforming *Int. J. Hydrog. Energy* **35** 7898–904

[48] Lazar M D, Dan M, Mihet M, Almasan V, Rednic V and Borodi G 2011 Hydrogen production by low temperature methane steam reforming using Ag and Au modified alumina supported nickel catalysts *Revue Roumaine de Chimie* **56** 637–42 (available at: http://revroum.lew.ro/wp-content/uploads/2011/RRCh_6_2011/Art%2011.pdf)

[49] Dan M, Mihet M, Biris A R, Marginean P, Almasan V, Borodi G, Watanabe F, Biris A S and Lazar M D 2012 Supported nickel catalysts for low temperature methane steam reforming: comparison between metal additives and support modification *React. Kinet. Mech. Catal.* **105** 173–93

[50] Maniecki T P, Stadnichenko A I, Maniukiewicz W, Bawolak K, Mierczyński P, Boronin A I and Jozwiak W K 2010 An active phase transformation on surface of Ni-Au/Al_2O_3 catalyst during partial oxidation of methane to synthesis gas *Kinet. Catal.* **51** 573–8

[51] Wang J, Lu X G, Sundman B and Su X 2005 Thermodynamic assessment of the Au–Ni system *Calphad Comput. Coupling Phase Diagrams Thermochem* **29** 263–8

[52] de Oliveira Rocha K, Marques C M P and Bueno J M C 2019 Effect of Au doping of Ni/Al_2O_3 catalysts used in steam reforming of methane: mechanism, apparent activation energy, and compensation effect *Chem. Eng. Sci.* **207** 844–52

[53] Xu Y, Lausche A C, Wang S, Khan T S, Abild-Pedersen F, Studt F, Nørskov J K and Bligaard T 2013 In silico search for novel methane steam reforming catalysts *New J. Phys.* **15** 125021

[54] Tomishige K, Li D, Tamura M and Nakagawa Y 2017 Nickel–iron alloy catalysts for reforming of hydrocarbons: preparation, structure, and catalytic properties *Catal. Sci. Technol.* **7** 3952–79

[55] Reddy G K and Smirniotis P G 2015 *Water Gas Shift Reaction: Research Developments and Applications* (Amsterdam: Elsevier) (https://doi.org/10.1016/C2013-0-09821-0)

[56] Schumacher N, Boisen A, Dahl S, Gokhale A A, Kandoi S, Grabow L C, Dumesic J A, Mavrikakis M and Chorkendorff I 2005 Trends in low-temperature water–gas shift reactivity on transition metals *J. Catal.* **229** 265–75

[57] Fajín J L C and Gomes J R B 2018 Water gas shift reaction promoted by bimetallic catalysts: an experimental and theoretical overview *Encyclopedia of Interfacial Chemistry: Surface Science and Electrochemistry* (Amsterdam: Elsevier) pp 314–8

[58] Gokhale A A, Dumesic J A and Mavrikakis M 2008 On the mechanism of low-temperature water gas shift reaction on copper *J. Am. Chem. Soc.* **130** 1402–14

[59] Fajín J L C, Cordeiro M N D S, Illas F and Gomes J R B 2009 Influence of step sites in the molecular mechanism of the water gas shift reaction catalyzed by copper *J. Catal.* **268** 131–41

[60] Liu P and Rodriguez J A 2007 Water-gas-shift reaction on metal nanoparticles and surfaces *J. Chem. Phys.* **126** 164705

[61] Yahiro H, Murawaki K, Saiki K, Yamamoto T and Yamaura H 2007 Study on the supported Cu-based catalysts for the low-temperature water–gas shift reaction *Catal. Today* **126** 436–40

[62] Rhodes C and Hutchings G J 2003 Studies of the role of the copper promoter in the iron oxide/chromia high temperature water gas shift catalyst *Phys. Chem. Chem. Phys.* **5** 2719

[63] Puig-Molina A, Cano F M and Janssens T V W 2010 The Cu promoter in an iron–chromium–oxide based water–gas shift catalyst under industrial conditions studied by *in-situ* XAFS *J. Phys. Chem.* C **114** 15410–6

[64] Estrella M, Barrio L, Zhou G, Wang X, Wang Q, Wen W, Hanson J C, Frenkel A I and Rodriguez J A 2009 *In situ* characterization of $CuFe_2O_4$ and Cu/Fe_3O_4 water–gas shift catalysts *J. Phys. Chem.* C **113** 14411–7

[65] Zhang Z, Wang -S-S, Song R, Cao T, Luo L, Chen X, Gao Y, Lu J, Li W-X and Huang W 2017 The most active Cu facet for low-temperature water gas shift reaction *Nat. Commun.* **8** 488

[66] Fajín J L C, Cordeiro M N D S, Illas F and Gomes J R B 2014 Generalized Brønsted–Evans–Polanyi relationships and descriptors for O–H bond cleavage of organic molecules on transition metal surfaces *J. Catal.* **313** 24–33

[67] Schweitzer N M, Schaidle J A, Ezekoye O K, Pan X, Linic S and Thompson L T 2011 High activity carbide supported catalysts for water gas shift *J. Am. Chem. Soc.* **133** 2378–81

[68] Phatak A A, Koryabkina N, Rai S, Ratts J L, Ruettinger W, Farrauto R J, Blau G E, Delgass W N and Ribeiro F H 2007 Kinetics of the water–gas shift reaction on Pt catalysts supported on alumina and ceria *Catal. Today* **123** 224–34

[69] Panagiotopoulou P and Kondarides D I 2006 Effect of the nature of the support on the catalytic performance of noble metal catalysts for the water–gas shift reaction *Catal. Today* **112** 49–52

[70] Ang M L, Miller J T, Cui Y, Mo L and Kawi S 2016 Bimetallic Ni–Cu alloy nanoparticles supported on silica for the water-gas shift reaction: activating surface hydroxyls via enhanced CO adsorption *Catal. Sci. Technol.* **6** 3394–409

[71] Saw E T, Oemar U, Tan X R, Du Y, Borgna A, Hidajat K and Kawi S 2014 Bimetallic Ni–Cu catalyst supported on CeO_2 for high-temperature water–gas shift reaction: methane suppression via enhanced CO adsorption *J. Catal.* **314** 32–46

[72] Arbeláez O, Reina T R, Ivanova S, Bustamante F, Villa A L, Centeno M A and Odriozola J A 2015 Mono and bimetallic Cu-Ni structured catalysts for the water gas shift reaction *Appl. Catal.* A **497** 1–9

[73] Jha A, Jeong D-W, Jang W-J, Rode C V and Roh H-S 2015 Mesoporous $NiCu–CeO_2$ oxide catalysts for high-temperature water–gas shift reaction *RSC Adv.* **5** 1430–7

[74] Lin J-H and Guliants V V 2012 Alumina-supported Cu@Ni and Ni@Cu core–shell nanoparticles: synthesis, characterization, and catalytic activity in water–gas-shift reaction *Appl. Catal.* A **445–6** 187–94

[75] Pastor-Pérez L, Gu S, Sepúlveda-Escribano A and Reina T R 2019 Bimetallic Cu–Ni catalysts for the WGS reaction—cooperative or uncooperative effect? *Int. J. Hydrog. Energy* **44** 4011–9

[76] Guo L, Li A, An X, Cao Z and Liu N 2015 Catalytic activity of $TM@Cu_{12}$ core–shell nanoclusters for water gas shift reaction *Int. J. Hydrog. Energy* **40** 8330–40

[77] Kozuch S and Shaik S 2011 How to conceptualize catalytic cycles? The energetic span model *Acc. Chem. Res.* **44** 101–10

[78] Luo W, Chen Y, Du Z and Chen C 2018 Theoretical study on $PdCu/CeO_2$ -catalyzed water–gas shift reaction: crucial role of the metal/ceria interface and O_2 enhancement effects *J. Phys. Chem.* C **122** 28868–83

[79] Saqlain M A, Hussain A, Siddiq D M, Leenaerts O and Leitão A A 2016 DFT study of synergistic catalysis of the water-gas-shift reaction on Cu–Au bimetallic surfaces *ChemCatChem* **8** 1208–17

[80] Ghosh S, Hariharan S and Tiwari A K 2017 Water adsorption and dissociation on copper/nickel bimetallic surface alloys: effect of surface temperature on reactivity *J. Phys. Chem.* C **121** 16351–65

[81] Fajín J L C, Cordeiro M N D S and Gomes J R B 2012 Water dissociation on bimetallic surfaces: general trends *J. Phys. Chem.* C **116** 10120–8

[82] Fajín J L C, Cordeiro M N D S, Illas F and Gomes J R B 2010 Descriptors controlling the catalytic activity of metallic surfaces toward water splitting *J. Catal.* **276** 92–100

[83] Fajín J L C, Cordeiro M N D S and Gomes J R B 2017 Water dissociation on multimetallic catalysts *Appl. Catal.* B **218** 199–207

[84] Boumaza S, Auroux A, Bennici S, Boudjemaa A, Trari M, Bouguelia A and Bouarab R 2010 Water gas shift reaction over the CuB_2O_4 spinel catalysts *React. Kinet. Mech. Catal.* **100** 145–51

[85] Fajín J L C and Cordeiro M N D S 2021 Insights into the catalytic activity of trimetallic Al/Zn/Cu surfaces for the water gas shift reaction *Appl. Surf. Sci.* **542** 148589

[86] Thouchprasitchai N, Luengnaruemitchai A and Pongstabodee S 2013 Water-gas shift reaction over Cu–Zn, Cu–Fe, and Cu–Zn–Fe composite-oxide catalysts prepared by urea-nitrate combustion *J. Ind. Eng. Chem.* **19** 1483–92

[87] Khan A, Chen P, Boolchand P and Smirniotis P G 2008 Modified nano-crystalline ferrites for high-temperature WGS membrane reactor applications *J. Catal.* **253** 91–104

[88] Natesakhawat S, Wang X, Zhang L and Ozkan U S 2006 Development of chromium-free iron-based catalysts for high-temperature water-gas shift reaction *J. Mol. Catal.* A **260** 82–94

[89] Burch R 2006 Gold catalysts for pure hydrogen production in the water–gas shift reaction: activity, structure and reaction mechanism *Phys. Chem. Chem. Phys.* **8** 5483–500

[90] Zhai Y *et al* 2010 Alkali-stabilized $Pt-OH_x$ species catalyze low-temperature water-gas shift reactions *Science* **329** 1633–6

[91] Jacobs G, Williams L, Graham U, Thomas G A, Sparks D E and Davis B H 2003 Low temperature water–gas shift: *in situ* DRIFTS-reaction study of ceria surface area on the evolution of formates on Pt/CeO_2 fuel processing catalysts for fuel cell applications *Appl. Catal.* A **252** 107–18

[92] Bunluesin T, Gorte R J and Graham G W 1998 Studies of the water-gas-shift reaction on ceria-supported Pt, Pd, and Rh: implications for oxygen-storage properties *Appl. Catal.* B **15** 107–14

[93] Iida H, Kondo K and Igarashi A 2006 Effect of Pt precursors on catalytic activity of Pt/TiO_2 (rutile) for water gas shift reaction at low-temperature *Catal. Commun.* **7** 240–4
[94] Panagiotopoulou P, Christodoulakis A, Kondarides D I and Boghosian S 2006 Particle size effects on the reducibility of titanium dioxide and its relation to the water–gas shift activity of Pt/TiO_2 catalysts *J. Catal.* **240** 114–25
[95] González I D, Navarro R M, Wen W, Marinkovic N, Rodriguéz J A, Rosa F and Fierro J L G 2010 A comparative study of the water gas shift reaction over platinum catalysts supported on CeO_2, TiO_2 and Ce-modified TiO_2 *Catal. Today* **149** 372–9
[96] Kalamaras C M, Americanou S and Efstathiou A M 2011 'Redox' vs 'associative formate with—OH group regeneration' WGS reaction mechanism on Pt/CeO_2: effect of platinum particle size *J. Catal.* **279** 287–300
[97] Kalamaras C M, Gonzalez I D, Navarro R M, Fierro J L G and Efstathiou A M 2011 Effects of reaction temperature and support composition on the mechanism of water–gas shift reaction over supported-Pt catalysts *J. Phys. Chem.* C **115** 11595–610
[98] Aragao I B, Ro I, Liu Y, Ball M, Huber G W, Zanchet D and Dumesic J A 2018 Catalysts synthesized by selective deposition of Fe onto Pt for the water-gas shift reaction *Appl. Catal.* B **222** 182–90
[99] Sener C, Wesley T S, Alba-Rubio A C, Kumbhalkar M D, Hakim S H, Ribeiro F H, Miller J T and Dumesic J A 2016 PtMo bimetallic catalysts synthesized by controlled surface reactions for water gas shift *ACS Catal.* **6** 1334–44
[100] Palma V and Martino M 2017 Pt-Re based catalysts for the realization of a single stage water gas shift process *Chem. Eng. Trans.* **57** 1657–62
[101] del Villar V, Barrio L, Helmi A, Annaland M V S, Gallucci F, Fierro J L G and Navarro R M 2016 Effect of Re addition on the WGS activity and stability of Pt/CeO_2–TiO_2 catalyst for membrane reactor applications *Catal. Today* **268** 95–102
[102] Azzam K G, Babich I V, Seshan K, Mojet B L and Lefferts L 2013 Stable and efficient Pt–Re/TiO_2 catalysts for water-gas-shift: on the effect of rhenium *ChemCatChem* **5** 557–64
[103] Duke A S, Xie K, Brandt A J, Maddumapatabandi T D, Ammal S C, Heyden A, Monnier J R and Chen D A 2017 Understanding active sites in the water–gas shift reaction for Pt–Re catalysts on Titania *ACS Catal.* **7** 2597–606
[104] Brandt A J, Maddumapatabandi T D, Shakya D M, Xie K, Seuser G S, Farzandh S and Chen D A 2019 Water-gas shift activity on Pt-Re surfaces and the role of the support *J. Chem. Phys.* **151** 234714
[105] Godbey D J and Somorjai G A 1988 The adsorption and desorption of hydrogen and carbon monoxide on bimetallic Re-Pt(111) surfaces *Surf. Sci.* **204** 301–18
[106] Godbey D J, Garin F and Somorjai G A 1989 The hydrogenolysis of ethane over Re-Pt(111) and Pt-Re(0001) bimetallic crystal surfaces *J. Catal.* **117** 144–54
[107] Detwiler M D, Majumdar P, Gu X-K, Delgass W N, Ribeiro F H, Greeley J and Zemlyanov D Y 2015 Characterization and theory of Re films on Pt(111) grown by UHV-CVD *Surf. Sci.* **640** 2–9
[108] Pettersson L and Sjöström K 1991 Decomposed methanol as a fuel—a review *Combust. Sci. Technol.* **80** 265–303
[109] Frei M S, Mondelli C, Short M I M and Pérez-Ramírez J 2020 Methanol as a hydrogen carrier: kinetic and thermodynamic drivers for its CO_2-based synthesis and reforming over heterogeneous catalysts *ChemSusChem* **13** 6330–7
[110] Stiles A B 1977 Methanol, past, present, and speculation on the future *AIChE J.* **23** 362–75
[111] Greeley J and Mavrikakis M 2004 Competitive paths for methanol decomposition on Pt(111) *J. Am. Chem. Soc.* **126** 3910–9
[112] Greeley J and Mavrikakis M 2002 A first-principles study of methanol decomposition on Pt(111) *J. Am. Chem. Soc.* **124** 7193–201
[113] Niu C-Y, Jiao J, Xing B, Wang G-C and Bu X-H2010 Reaction mechanism of methanol decomposition on Pt-based model catalysts: a theoretical study *J. Comput. Chem.* **31** 2023–37
[114] Kapoor M P, Ichihashi Y, Kuraoka K and Matsumura Y 2003 Catalytic methanol decomposition over palladium deposited on thermally stable mesoporous titanium oxide *J. Mol. Catal.* A **198** 303–8
[115] Matsumura Y, Tanaka K, Tode N, Yazawa T and Haruta M 2000 Catalytic methanol decomposition to carbon monoxide and hydrogen over nickel supported on silica *J. Mol. Catal.* A **152** 157–65
[116] Tsoncheva T, Ivanova L, Minchev C and Fröba M 2009 Cobalt-modified mesoporous MgO, ZrO_2, and CeO_2 oxides as catalysts for methanol decomposition *J. Colloid Interface Sci.* **333** 277–84
[117] Yuan D, Gong X and Wu R 2008 Decomposition pathways of methanol on the PtAu(111) bimetallic surface: a first-principles study *J. Chem. Phys.* **128** 064706
[118] Matolín V, Johánek V, Škoda M, Tsud N, Prince K C, Skála T and Matolínová I 2010 Methanol adsorption and decomposition on $Pt/CeO_2(111)/Cu(111)$ thin film model catalyst *Langmuir* **26** 13333–41
[119] Sexton B A 1981 Methanol decomposition on platinum (111) *Surf. Sci.* **102** 271–81
[120] Cao D, Lu G Q, Wieckowski A, Wasileski S A and Neurock M 2005 Mechanisms of methanol decomposition on platinum: a combined experimental and *ab initio* approach *J. Phys. Chem.* B **109** 11622–33
[121] Miller A V, Kaichev V V, Prosvirin I P and Bukhtiyarov V I 2013 Mechanistic study of methanol decomposition and oxidation on Pt(111) *J. Phys. Chem.* C **117** 8189–97
[122] Levis R J, Zhicheng J, Winograd N, Akhter S and White J M 1988 Methyl formation from methanol decomposition on Pd{111} and Pt{111} *Catal. Lett.* **1** 385–9
[123] Wang J and Masel R I 1991 C-O bond scission during methanol decomposition on (1×1)Pt(11O) *J. Am. Chem. Soc.* **113** 5850–6
[124] Motoo S and Furuya N 1985 Electrochemistry of platinum single crystal surfaces. Part II. Structural effect on formic acid oxidation and poison formation on Pt (111), (100) and (110) *J. Electroanal. Chem.* **184** 303–16
[125] Shao Y, Yin G and Gao Y 2007 Understanding and approaches for the durability issues of Pt-based catalysts for PEM fuel cell *J. Power Sources* **171** 558–66
[126] Du P, Wu P and Cai C 2015 Mechanistic insight into the facet-dependent adsorption of methanol on a Pt_3Ni nanocatalyst *J. Phys. Chem.* C **119** 18352–63
[127] Fajín J L C and Cordeiro M N D S 2021 Light alcohols reforming towards renewable hydrogen production on multicomponent catalysts *Renew. Sustain. Energy Rev.* **138** 110523
[128] Xu C, Su Y, Tan L, Liu Z, Zhang J, Chen S and Jiang S P 2009 Electrodeposited PtCo and PtMn electrocatalysts for methanol and ethanol electrooxidation of direct alcohol fuel cells *Electrochim. Acta* **54** 6322–6
[129] Luo J, Njoki P N, Lin Y, Mott D, Wang L and Zhong C J 2006 Characterization of carbon-supported AuPt nanoparticles for electrocatalytic methanol oxidation reaction *Langmuir* **22** 2892–8
[130] Xu J, Hua K, Sun G, Wang C, Lv X and Wang Y 2006 Electrooxidation of methanol on carbon nanotubes supported Pt–Fe alloy electrode *Electrochem. Commun.* **8** 982–6
[131] Guo W, Tian W Q, Lian X, Liu F, Zhou M, Xiao P and Zhang Y 2014 A comparison of the dominant pathways for the methanol dehydrogenation to CO on Pt_7 and $Pt_{7-x}Ni_x$ (x=1, 2, 3) bimetallic clusters: a DFT study *Comput. Theor. Chem.* **1032** 73–83

[132] McCabe R W and Schmidt L D 1977 Binding states of CO on single crystal planes of Pt *Surf. Sci.* **66** 101–24
[133] Ren H, Humbert M P, Menning C A, Chen J G, Shu Y, Singh U G and Cheng W C 2010 Inhibition of coking and CO poisoning of Pt catalysts by the formation of Au/Pt bimetallic surfaces *Appl. Catal.* A **375** 303–9
[134] Zhong W, Liu Y and Zhang D 2012 A comparative theoretical study for the methanol dehydrogenation to CO over Pt_3 and $PtAu_2$ clusters *J. Mol. Model.* **18** 3051–60
[135] Tenney S A, Islamuddin Shah S, Yan H, Cagg B A, Levine M S, Rahman T S and Chen D A 2013 Methanol reaction on Pt–Au clusters on TiO_2(110): methoxy-induced diffusion of Pt *J. Phys. Chem.* C **117** 26998–7006
[136] Tenney S A, Ratliff J S, Roberts C C, He W, Ammal S C, Heyden A and Chen D A 2010 Adsorbate-induced changes in the surface composition of bimetallic clusters: Pt–Au on TiO_2(110) *J. Phys. Chem.* C **114** 21652–63
[137] Damte J Y, Lyu S L, Leggesse E G and Jiang J C 2018 Methanol decomposition reactions over a boron-doped graphene supported Ru–Pt catalyst *Phys. Chem. Chem. Phys.* **20** 9355–63
[138] Ding Q, Xu W, Sang P, Xu J, Zhao L, He X and Guo W 2016 Insight into the reaction mechanisms of methanol on PtRu/Pt(111): a density functional study *Appl. Surf. Sci.* **369** 257–66
[139] Zhang S T, Yan H, Wei M, Evans D G and Duan X 2014 Hydrogenation mechanism of carbon dioxide and carbon monoxide on Ru(0001) surface: a density functional theory study *RSC Adv.* **4** 30241–9
[140] Zhao L, Wang S, Ding Q, Xu W, Sang P, Chi Y, Lu X and Guo W 2015 The oxidation of methanol on PtRu(111): a periodic density functional theory investigation *J. Phys. Chem.* C **119** 20389–400
[141] Mehmood F, Rankin R B, Greeley J and Curtiss L A 2012 Trends in methanol decomposition on transition metal alloy clusters from scaling and Brønsted–Evans–Polanyi relationships *Phys. Chem. Chem. Phys.* **14** 8644–52
[142] Strickland G 1984 Hydrogen derived from ammonia: small-scale costs *Int. J. Hydrog. Energy* **9** 759–66
[143] Hansgen D A, Vlachos D G and Chen J G 2010 Using first principles to predict bimetallic catalysts for the ammonia decomposition reaction *Nat. Chem.* **2** 484–9
[144] Wu H, Sutton J E, Guo W and Vlachos D G 2019 Volcano curves for in silico prediction of mono- and bifunctional catalysts: application to ammonia decomposition *J. Phys. Chem.* C **123** 27097–104
[145] Levy R B and Boudart M 1973 Platinum-like behavior of tungsten carbide in surface catalysis *Science* **181** 547–9
[146] Boudart M, Oyama S T and Leclercq L 1981 Molybdenum carbide, oxycarbide and nitride as catalysts in the activation of CO, N–N, C–C and H–H bonds *New Horizons in Catalysis—Proceedings of the 7th International Congress on Catalysis (Studies in Surface Science and Catalysis 7)* ed T Seivama and K Tanabe (Tokyo: Kodansha Ltd) pp 578–90
[147] Mukherjee S, Devaguptapu S V, Sviripa A, Lund C R F and Wu G 2018 Low-temperature ammonia decomposition catalysts for hydrogen generation *Appl. Catal.* B **226** 162–81
[148] Dulong P L and Thenard L J 1823 LVIII. Note on the property which some metals possess of facilitating the combination of elastic fluids *Philos. Mag.* **62** 282–6
[149] Robertson A J B 1975 The early history of catalysis *Platin. Met. Rev.* **19** 64–9 (available at: http://www.platinummetalsreview.com/pdf/pmr-v19-i2-064-069.pdf)
[150] Ganley J C, Thomas F S, Seebauer E G and Masel R I 2004 *A priori* catalytic activity correlations: the difficult case of hydrogen production from ammonia *Catal. Lett.* **96** 117–22
[151] Yin S F, Xu B Q, Zhou X P and Au C T 2004 A mini-review on ammonia decomposition catalysts for on-site generation of hydrogen for fuel cell applications *Appl. Catal.* A **277** 1–9
[152] Boisen A, Dahl S, Norskov J and Christensen C 2005 Why the optimal ammonia synthesis catalyst is not the optimal ammonia decomposition catalyst *J. Catal.* **230** 309–12
[153] Yin S F, Xu B Q, Zhu W X, Ng C F, Zhou X P and Au C T 2004 Carbon nanotubes-supported Ru catalyst for the generation of CO_x-free hydrogen from ammonia *Catal. Today* **93–95** 27–38
[154] Jacobsen C J H, Dahl S, Clausen B S, Bahn S, Logadottir A and Nørskov J K 2001 Catalyst design by interpolation in the periodic table: bimetallic ammonia synthesis catalysts *J. Am. Chem. Soc.* **123** 8404–5
[155] Duan X, Ji J, Qian G, Fan C, Zhu Y, Zhou X, Chen D and Yuan W 2012 Ammonia decomposition on Fe(110), Co(111) and Ni(111) surfaces: a density functional theory study *J. Mol. Catal.* A **357** 81–6
[156] Duan X, Qian G, Zhou X, Chen D and Yuan W 2012 MCM-41 supported Co Mo bimetallic catalysts for enhanced hydrogen production by ammonia decomposition *Chem. Eng. J.* **207–8** 103–8
[157] Ruban A V, Skriver H L and Nørskov J K 1999 Surface segregation energies in transition-metal alloys *Phys. Rev.* B **59** 15990–6000
[158] Hansgen D A, Thomanek L M, Chen J G and Vlachos D G 2011 Experimental and theoretical studies of ammonia decomposition activity on Fe-Pt, Co-Pt, and Cu-Pt bimetallic surfaces *J. Chem. Phys.* **134** 184701
[159] Menning C A and Chen J G 2008 Thermodynamics and kinetics of oxygen-induced segregation of *3d* metals in Pt–*3d*–Pt(111) and Pt–*3d*–Pt(100) bimetallic structures *J. Chem. Phys.* **128** 164703
[160] Menning C A and Chen J G 2009 General trend for adsorbate-induced segregation of subsurface metal atoms in bimetallic surfaces *J. Chem. Phys.* **130** 174709
[161] Menning C A and Chen J G 2010 Regenerating Pt–3d–Pt model electrocatalysts through oxidation–reduction cycles monitored at atmospheric pressure *J. Power Sources* **195** 3140–4
[162] Tao F *et al* 2010 Evolution of structure and chemistry of bimetallic nanoparticle catalysts under reaction conditions *J. Am. Chem. Soc.* **132** 8697–703
[163] Grass M E, Park M, Aksoy F, Zhang Y, Kunz M, Liu Z and Mun B S 2010 Effect of O_2, CO, and NO on surface segregation in a $Rh_{0.5}Pd_{0.5}$ bulk crystal and comparison to $Rh_{0.5}Pd_{0.5}$ nanoparticles *Langmuir* **26** 16362–7
[164] Brune H 1998 Microscopic view of epitaxial metal growth: nucleation and aggregation *Surf. Sci. Rep.* **31** 125–229
[165] Jiang Z, Qin P and Fang T 2016 Theoretical study of NH_3 decomposition on Pd-Cu(111) and Cu-Pd(111) surfaces: a comparison with clean Pd(111) and Cu(111) *Appl. Surf. Sci.* **371** 337–42
[166] Jiang Z and Fang T 2019 Probing the effect of Pd coverage towards NH_3 decomposition on Cu(100) surface *Chem. Phys. Lett.* **729** 30–6
[167] Novell-Leruth G, Valcárcel A, Pérez-Ramírez J and Ricart J M 2007 Ammonia dehydrogenation over platinum-group metal surfaces. Structure, stability, and reactivity of adsorbed NH_x species *J. Phys. Chem.* C **111** 860–8
[168] Huang C, Li H, Yang J, Wang C, Hu F, Wang X, Lu Z-H, Feng G and Zhang R 2019 $Ce_{0.6}Zr_{0.3}Y_{0.1}O_2$ solid solutions-supported NiCo bimetal nanocatalysts for NH_3 decomposition *Appl. Surf. Sci.* **478** 708–16
[169] Lucentini I, Casanovas A and Llorca J 2019 Catalytic ammonia decomposition for hydrogen production on Ni, Ru and Ni–Ru supported on CeO_2 *Int. J. Hydrog. Energy* **44** 12693–707

[170] Choudhary T V, Sivadinarayana C and Goodman D W 2001 Catalytic ammonia decomposition: CO_x-free hydrogen production for fuel cell applications *Catal. Lett.* **72** 197–201
[171] Vacharapong P, Arayawate S, Henpraserttae S, Katanyutanon S, Charojrochkul S, Lawtrakul L and Toochinda P 2019 Effect of magnetic inducement in preparation of Ni/Ce-doped Al_2O_3 for ammonia decomposition *ChemistrySelect* **4** 11913–9
[172] Yi Y, Wang L, Guo Y, Sun S and Guo H 2018 Plasma-assisted ammonia decomposition over Fe–Ni alloy catalysts for CO_x-free hydrogen *AIChE J.* **65** 691–701
[173] Xie P, Yao Y, Huang Z, Liu Z, Zhang J, Li T, Wang G, Shahbazian-Yassar R, Hu L and Wang C 2019 Highly efficient decomposition of ammonia using high-entropy alloy catalysts *Nat. Commun.* **10** 4011